Strength of eccentrically loaded slender columns made with high-strength concrete

Accepted manuscript doi:
10.1680/jstbu.19.00064

Accepted manuscript doi:
10.1680/jstbu.19.00064

Submitted: 15 March 2019

Published online in 'accepted manuscript' format: 21 August 2019

Manuscript title: Strength of eccentrically loaded slender columns made with high-strength concrete

Authors: Ibrahim G. Shaaban[1], Gamal T. Abdel-Rahman[2], Mohamed Said[2], Mahmoud Abdel-Karim[2] and Peter Adesina[3]

Affiliations: [1]Civil Engineering and Built Environment, School of Computing and Engineering, University of West London, UK; [2]Civil Engineering Department, Faculty of Engineering, Shoubra, Benha University, Egypt and [3]Department of Structural Engineering, Imperial College, London, UK

Corresponding author: Ibrahim G. Shaaban, Civil Engineering and Built Environment, School of Computing and Engineering, University of West London, UK.

E-mail: ibrahim.shaaban@uwl.ac.uk

Accepted manuscript doi:
10.1680/jstbu.19.00064

Abstract

A non-linear finite-element analysis model was developed to predict the strength analysis of high- strength-concrete slender columns. The studied parameters were compressive strength, load eccentricity, slenderness ratio, longitudinal and transverse reinforcement ratio. The model results were verified by comparison with analytical results and experimental results in literature. A parametric study was also carried out by comparing the model results with those obtained using design codes, which were predominantly based on data derived from tests on normal-strength concrete. The model proved to be a suitable tool for the strength analysis of slender high-strength-concrete columns. ACI-318-14 gave the most conservative predictions of the load-carrying capacity of centrally loaded columns but was close to the model results for eccentric loading. The procedures specified by BS EN 1992-1-1:2004 Eurocode 2 resulted in a significant under-estimation of the load-carrying capacity of slender columns, particularly for eccentric loading, and this increases with greater slenderness ratios. This is probably because the confinement index taken into consideration in the software was not consistent, ranging from 0.03% to 5.14%. It was concluded that special clauses need to be introduced in design codes for the accurate design of high-strength-concrete columns.

Keywords: Finite element method; Codes of practice & standards; Columns; Stress analysis

Accepted manuscript doi:
10.1680/jstbu.19.00064

1. Introduction

In recent years, there has been a rapid increase of using high-strength concrete (HSC) in structural elements, especially columns, due to their better performance behaviour compared with normal-strength concrete (NSC). The Concrete Society defined HSC as concrete with a specified characteristic cube strength between 60 and 100 N/mm^2. The significance of the slenderness effects in high strength concrete (HSC) slender columns raised a question about the adequacy of current building design codes, predominantly based on data derived from tests on NSC, to be adopted for the design of HSC columns (Beal and Khalil, 1999; Angus, 2007). Slenderness ratio is the ratio of the effective length of a column (L_e) and the least radius of gyration (r) about the axis under consideration. It is given by the symbol 'λ' (lambda). Methods used in the strength analysis of slender columns found in the literature, based on a simplified non-linear analysis, generally ignored the beneficial influence of the concrete core confinement effect on column Behaviour (Galeota, Giammatteo and Marino, 1992). Kim and Yang (1995) concluded that the ultimate load for slender columns depends mainly on the flexural rigidity rather than the axial rigidity. Consequently, the effect of the load eccentricity ratio (e/h) and slenderness ratio (λ) on columns could be captured by the neutral axis depth. As the neutral axis depth decreased a lower load-carrying capacity and a higher ductility will be expected for eccentric columns.

Lee and Son (2000) reported that medium length columns with a slenderness ratio of 40 failed in tension and in a relatively more ductile manner than the short columns with a slenderness ratio of 19 under the same initial eccentricities. Furthermore, long columns with a slenderness ratio of 61 failed in a more ductile manner than the short and medium length columns. This is probably due to the fact that the column moment gradient of the long column is greater than that of the short column due to the P-Delta effect. In addition, the stress-strain models for unconfined concrete adopted by the available methods influence modeling errors (Zhou and Hong, 2001). Ignoring confinement effect has been reported to result in an overly conservative post-peak response of the columns (Niu and Cao, 2015; Elchalakani, Aslani and Duan, 2017). Soliman (2011) studied the Behaviour of long confined slender concrete columns confined by proper plastic tube (FRP). He reported that the effect of column confinement on the compressive strength of the columns was enhanced as the slenderness ratio reduced. Ratio of axial strain in confined columns to that in unconfined column was found to decrease as slenderness ratio increases while radial strain ratio was found to increase with increasing column slenderness ratio. Abdel-Karim et al. (2017) developed a theoretical model, based on a stability analysis of pin-ended columns, for the analysis of the long column Behaviour taking tension-stiffening effect into consideration. Their prediction of the ultimate loads correlated very well with experimental values from literature.

Kottb et al. (2015) employed analytical and experimental programs to study the Behaviour of HSC columns subjected to eccentric compression. They tested 10 square columns subjected to load eccentricity, column slenderness ratio, and ratios of longitudinal and transverse reinforcement, experimentally. In addition, they carried out a parametric study for nineteen columns to understand how the study parameters influence the theoretical Behaviour of studied columns. NLFEA results were in good agreement with the experimental values especially in columns with moderate reinforcement. All studied columns generally exhibited analytical capacities less than the experimental values with an average difference of 16% and 17% for column ultimate load and mid-height deflection, respectively. They showed that increasing slenderness ratio results in an increase in the mid-height deflection, subsequently

the bending moments at column mid-height increased causing a reduction in the depth of compressed zone. Foster et al. (1997); Brown (2012); Li et al. (2017) reported that decreasing the tie spacing (increasing the transverse reinforcement ratio) improves the column confinement and consequently enhances the column capacity and ductility. This enhancement was noticed mainly at concentric columns with low concrete compressive strength, while it diminished by increasing the load eccentricity ratio or the slenderness ratio. Higher confinement efficiency is exhibited by lower strength concrete due to larger deformability of such concrete. In contrast, Canbay, Ozcebe and Ersoy (2006) reported that increasing stirrup sizes was also found effective in enhancing HSC column capacity as the columns failed at higher loads. Niu and Cao (2015) reported that the incorporation of reinforcement cage made of longitudinal reinforcement and transverse stirrups resulted in an increase in the ultimate strength of steel tubular columns. Column enhancement effectiveness was also found to be greatly influenced by the geometric factors of a column and reduced with increasing aspect ratio by Li et al. (2017).

2. Research Objective

In this research, a non-linear finite element model was developed for the strength prediction of eccentrically loaded HSC slender columns. The model was developed using a general-purpose computer package 'Ansys 13.0' (Ansys, 2009). The results obtained by the finite element model developed in this paper are verified by comparisons with theoretical results obtained by (Abdel-Karim et al., 2017) and experimental results from literature (Lloyd and Rangan, 1996; Lee and Son, 2000; Foster et al, 1997). In addition, a parametric study was carried out to compare the results obtained by the finite element model with those obtained by the current design codes of practice, ECP-203; ACI-318-14; BS EN 1992-1-1:2004 Eurocode 2. The ultimate objective of this research is to develop a finite element model and to incorporate it in a NLFEA Ansys package as an accurate tool for the analysis and design of HSC slender and or eccentric columns. This, in turn, will be a step on the way to introduce new clauses in the design codes to predict the strength of HSC slender columns more accurately.

3. NLFEA using Ansys

Different studies were carried out to investigate the analysis of HSC structural elements using finite element models using the Ansys package. Wu et al. (2009) studied HSC circular columns confined by aramid fiber-reinforced polymer sheets. Antony et al. (2013) developed a finite element model for the prediction of the shear strength of concrete deep beam. Reddy et al. (2015) carried out finite element analysis of HSC beams in shear. In the current investigation, the authors firstly developed a numerical model using Ansys and then applied it to experimentally tested column specimens to verify the results predicted by the model. Ansys modeling was used later for a parametric study to compare the numerical results with those obtained by the available design codes.

3.1 Material and Geometrical Modeling of Studied Specimens

Non-linear finite element modelling of the HSC columns using Ansys 13.0 (Ansys, 2009) was conducted to simulate HSC elements using 3-D isoparametric elements, Solid 65 to simulate the concrete; while the line element, 3D-Link180 was adopted to idealise the reinforcing bars (see Figure 1). A very rigid loading plate of 3-D isoparametric elements, Solid 385 was used under the eccentric concentrated loads to simulate the actual load distribution avoiding the local failure. Both linear and non-linear behaviours of the concrete were considered. Cracking or crushing of Solid 65 is initiated once one of the element

principal stresses, at an element integration point, exceeds the tensile or compressive strength of the concrete. Cracked or crushed regions, as opposed to discrete cracks, are then formed perpendicular to the relevant principal stress direction with stresses being redistributed locally. The element is thus nonlinear and requires an iterative solver. In the numerical routines, the formation of a crack is achieved by the modification of the stress-strain relationships of the element to introduce a plane of weakness in the requisite principal stress direction. Typical shear transfer coefficient ranges from 0.0 to 1.0, with zero-value representing a very smooth crack and 1.0 representing a very rough crack. This feature may be applied for both the open and closed crack. Shear transfer coefficients were taken as 0.2 for open crack and 0.8 for closed crack. A value of 0.6 for stress relaxation after cracking was considered in the analysis. These values revealed accepted Behaviour for the investigated columns according to the correlative study conducted. Details of the shear transfer coefficient is reported elsewhere (Habasaki, 2000). The complete nonlinear material modeling is detailed elsewhere. (Abdel-Karim, 2016).

The stress-strain curve developed by Attard and Setunge (1996) for unconfined high-strength concrete (see Figure 2) was adopted as follows:

$$f_c = \alpha f_c' \left[\frac{A\left(\frac{\varepsilon_c}{\varepsilon_{co}}\right) + B\left(\frac{\varepsilon_c}{\varepsilon_{co}}\right)^2}{1 + (A-2)\left(\frac{\varepsilon_c}{\varepsilon_{co}}\right) + (B+1)\left(\frac{\varepsilon_c}{\varepsilon_{co}}\right)^2} \right] \quad (1)$$

For the ascending curve parameters,

$$A = ((E_c \varepsilon_{co})/f_c')\,; \quad B = (A-1)^2/(0.55) - 1 \quad (2)$$

and for the descending curve parameters,

$$A = [f_{ic}\,(\varepsilon_{ic} - \varepsilon_{c0})^2]/[(f_c - f_{ic})(\varepsilon_{c0}\varepsilon_{ic})]\,; \quad B = 0 \quad (3)$$

where

$$\varepsilon_{co} = \frac{4.26\, f_c'}{E_c \sqrt[4]{f_c'}}(\text{MPa}); \quad (4)$$

$$E_c = \left(3320\sqrt{f_c'} + 6900\right)(\text{MPa}); \quad (5)$$

$$\varepsilon_{ic} = \left(2.5 - 0.3\, ln(f_c')\right)\varepsilon_{c0}(\text{MPa}); \quad (6)$$

$$f_{ic} = \left(1.41 - 0.171\, ln(f_c')\right)f_c'(\text{MPa}); \quad (7)$$

f_c' is the unconfined concrete compressive strength; α is a factor to account for the size effect taken as 0.85 as recommended by Foster, Liu and Sheikh (1998); and Ec is the concrete modulus of elasticity. The steel reinforcement was modeled by 3D-Link180 element as mentioned above (see Figure 1b). It is a uniaxial tension-compression element with three degrees of freedom at each node, translation in the nodal x, y, and z directions. As in a pin-jointed structure, the element is not capable of carrying bending moments or twist loads. The stress assumed to be constant along the entire length. The inherent assumption is that there is full displacement compatibility between the reinforcement and the concrete and that no bond slippage occurs. The plasticity model used is rate independent isotropic hardening plasticity where the yield surface size changes, but the center axis and the general shape of the yield surface do not change. The uniform expansion of the yield surface can also be seen on a stress-strain diagram of an isotropic hardening Behaviour; the compressive and tensile yield strengths are increasing together by the same amount. Bilinear stress-strain curve was used to idealise the

characteristics of steel reinforcement as shown in Figure 3. The stress-strain relationship is expressed by two linear equations as follows:

For $\varepsilon_s \leq \varepsilon_y$

$$f_s = E_s \varepsilon_s; \quad (8)$$

and for $\varepsilon_s \geq \varepsilon_y$

$$f_s = E_s \varepsilon_s + \frac{E_s}{100}(\varepsilon_s - \varepsilon_y) \quad (9)$$

where f_s and ε_s are the average stress and strain of the steel bars, respectively; f_y and ε_y are the yield stress and strain of steel bars, respectively; E_s is the Young's Modulus of steel reinforcement.

The columns were analyzed as simply supported along the ends. All columns were modeled considering the advantage of symmetry at the column mid-height to reduce the computational time. The boundary conditions and the modelling of supports were applied to one-half of the modelled columns as shown in Figure 4. This is similar to the idealisation of columns presented by Kottb et al., 2015. The numerical solution scheme adopted for non-linear analysis was performed in several load steps refined towards the peak load. Each load step was divided into incremental load sub-steps, where the number of sub-steps was automatically determined based on a minimum sub-step of 30 and a maximum of 200. For each load increment, the iterative solution was performed using modified Newton-Raphson method in which the stiffness was regularly reformulated. Convergence criterions were achieved by two methods; displacement-controlled solution, and force-controlled solution, with a maximum convergence tolerance of 2%. The convergence tolerance was relaxed for few column specimens to be 5%. The load level at which the convergence criterion was not fulfilled, indicating numerical instability, was regarded as the analytical failure load of the column specimen. It is worth mentioning that both of material and geometrical nonlinearity were taken into account in the NLFEA. It is obvious that increasing the column's free height without changing the cross section resulted in reduction of ultimate loads and that's why the geometrical nonlinearity affects the results of slender columns.

3.2 Analyzed Column Specimens

A total of 74 column specimens, experimentally tested in literature, were modeled and compared with results of NLFEA. These experimentally tested specimens are detailed herein. Fifteen eccentrically loaded HSC columns were selected from the experimental tests carried out by Lloyd and Rangan (1996) for comparison purposes. The studied columns had dimensions of 175 x175mm with a constant length of 1500mm. The main studied variables were concrete compressive strength (60, 92, and 97 MPa), longitudinal reinforcement ratio (1.5% and 2%), and load eccentricity (15, 50, and 65 mm). Characteristics of the above-mentioned column specimens are reported in Table 1 along with predictions carried out using NLFEA model. Among the columns tested by Lee and Son (2000), 23 columns specimens were selected to investigate the structural Behaviour and strength of eccentrically loaded reinforced concrete tied columns. The columns dimensions were 120 x120 mm at the mid-section. Main variables included were concrete compressive strength (70, and 93 MPa), longitudinal reinforcement ratio (2% and 5%), eccentricity range (20 to 65 mm), and column height (660, 1380, and 2100 mm). The details of the test specimens along with predictions by NLFEA are reported in Table 2. From the experimental program presented by Foster et al.

(1997), 36 eccentrically loaded HSC columns were chosen. The columns were 150 x150 mm at the mid-section and hunched at the ends to apply the eccentric loading and prevent boundary effects. Concrete strengths were 75, and 90 MPa with load eccentricities of 8, 20, and 50 mm. The columns had either 2% or 4% longitudinal reinforcement. The tie spacing was either 30, 60, or 120 mm. Details of the specimens and comparisons with NLFEA results are reported in Table 3.

4. NLFEA Predictions

The following sections present verification of the NLFEA results by comparisons with the results obtained by experimental results carried out by Lloyd and Rangan, 1996; Lee and Son, 2000; Foster et al, 1997, and the analytical model developed earlier by the authors (Abdel-Karim et al.,2017). Column load-carrying capacities and mid-height deflections were used as the parameters for comparison. The experimental results and predicted values are reported in Tables 1-3. Table 1 shows the ultimate capacities and corresponding deflections at mid-height of the fifteen column specimens experimentally tested by Lloyd and Rangan (1996) and predicted by the developed NLFEA model. It can be seen from Table 1 that, generally, the NLFEA results under-estimated the peak load of all columns tested by Lloyd and Rangan (1996), especially columns having eccentricity ratio of about 0.1. Enhanced load-carrying capacities were obtained for columns with eccentricity ratio of 0.29 and 0.37. In addition, NLFEA model considerably under-estimated the mid-height deflection for all column specimens at failure. However, Table 1 shows good agreement between the experimental results and the prediction by the NLFEA with an average ratio of 0.86. Figure 5 shows that there is a reasonable agreement between the experimental load-deflection curves obtained by Lloyd and Rangan (1996) at columns mid-height and the corresponding NLFEA curves for selective specimens of ultimate values reported in Table 1.

Table 2 shows, generally, that NLFEA overestimated the columns tested by Lee and Son (2000) while Table 3 shows that NLFEA model under-estimated the mid-height deflection for columns tested by Foster et al. (1997). For instance, Columns HS2 in Table 2 and Column 2M50-60 in Table 3, which practically had same paramters including concrete compressive strength, longitudinal reinforcement ratio, loading eccentricity, and slenderness ratio, experienced distinct mid-hieght deflection of 2.8 and 8.4 mm, respectively. This may be attributed to the column imperfections and material variability which can affect the prediction of mid-height deflection. This is in agreement with Li et al., (2017) who found that the quality and relevance of experimental data is highly influential in evaluating the performance of NLFEA. Figure 6a shows correlation between the experimental mid-height deflections of columns with the predictions of NLFEA. The NLFEA of the column model showed higher stiffness compared with the experimentally tested columns. Figure 6b illustrates the correlation between the predicted normalised column load-carrying capacities with experimental results. It can be seen from Figure 6b that the experimental results are in close agreement to results obtained by NLFEA. In addition, Figure 7 presents output samples for NLFEA of Column HM3 (experimentally tested by Lee and Son (2000) indicating the cracks propagation, deformed shape and column concrete stresses.

4.1 Effect of Concrete Compressive Strength

HSC columns are more brittle than Normal Strength Concrete (NSC) and suffer early cover spalling. Increasing the concrete compressive strength of columns, therefore, reduces column confinement. Subsequently, the normalised capacity of HSC columns is reduced by

Accepted manuscript doi:
10.1680/jstbu.19.00064

increasing concrete compressive strength. Normalised ultimate loads for tested specimens were extracted from Tables 1-3 and they were plotted against studied parameters such as eccentricity, slenderness, confinement, and compressive strength in Figure 8. The reduction in the normalised load-carrying capacity is dependent on the strain gradient developed either by the load eccentricity (Figure 8a) or by the column slenderness ratio (Figure 8b). As the strain gradient increases, the effect of the concrete compressive strength on the normalised load-carrying capacity is diminished. It can be seen from Figure 8a that increasing the concrete compressive strength from 58 MPa to 97 MPa lead to a gradual reduction of the normalised load-carrying capacity, predicted by the NLFEA for columns with e/h of 0.09 and 0.29 by 5%, and 3%, respectively. In general, the NLFEA slightly under-estimated the normalised load-carrying capacity for eccentric columns with $e/h \leq 0.1$, and provided with congested reinforcement cage ($S = 30mm$ or $\rho_s = 4\%$) (see Figure 8c). It can be argued that the NLFEA model does not consider early spalling of concrete cover.

4.2 Effect of Load Eccentricity and Slenderness Ratio

Figures 9a and b extracted the normalised ultimate loads from Tables 1 and 3 for specimens tested by Lloyd and Rangan (1996) and (Foster et al. (1997), respectively. These figures show the effect of load eccentricity on the normalised load-carrying capacity at constant slenderness ratio, λ of 30 and 15, respectively. Figure 9b shows that the prediction of normalised load-carrying capacity depends on the tie spacing, where reducing the tie spacing increases the normalised load-carrying capacity. The confinement enhancement due to decreasing the tie spacing was reduced by increasing the load eccentricity ratio. The reduction reported in experimental investigations for the normalised load-carrying capacity for columns having 30 mm tie spacing was justified by the early separation of concrete cover due to the congested reinforced cage that generate a weakened plane between the cover and the confined core (Foster et al., 1997). Afefy and El-Tony (2016) reported that providing end eccentricities to columns resulted in a reduction in the axial capacity and this reduction is dependent on the value of the end eccentricity. It can be observed from Figures 9a, b, and Table 2 that NLFEA model slightly under-estimated the contribution of the column confinement. Reducing the tie spacing from 120mm to 60mm (increasing the transverse reinforcement volumetric ratio from 0.69% to 1.38%) resulted in an increase in the experimental normalised load-carrying capacity by approximately 15%. Figure 9b shows also that the columns with tie spacing of 30mm had normalised load-carrying capacity less than that for columns with 60mm tie spacing due to early spalling of concrete cover of highly confined columns.

Increasing the eccentricity ratio is shown to enhance the NLFEA results. For instance, it can be seen from Figure 9c and Table 2 that for Columns HS1 and HS2, increasing the eccentricity ratio from 0.21 to 0.38 resulted in P_{num}/P_{exp} from 0.9 to 0.98, respectively. However, NLFEA overestimated the normalised load-carrying capacity for columns having a high eccentricity ratio combined with a high slenderness ratio. This is clear from the results of Columns ‘HM3’, ‘HL2’ and ‘HL3’ as shown in Figure 9c and Table 2. Lloyd and Rangan (1996) reported that low confinement reinforcement ratios ≤ 0.4% were insufficient to produce ductile behaviour for columns with low load eccentricity ($e/h \leq 0.10$). The failure of such columns was sudden, brittle, and explosive. On the other hand, columns subjected to higher load eccentricities ($e/h \geq 0.30$) behaved in a more ductile manner (Foster et al., 1997; Ghoneim, 2002; Kottb et al., 2015). Figure 10 extracted the normalised ultimate loads from Table 2 for column specimens tested by Lee and Son (2000). Figure 10 shows the effect of the slenderness ratio on the column load-carrying capacity. It can be seen from the figure

Accepted manuscript doi:
10.1680/jstbu.19.00064

and Table 2 that NLFEA under-estimated the prediction of normalised load–carrying capacity for studied columns. For example, Columns, HS1, HM1, and HL1 had ($P_{num}/P_{exp} = 0.9, 0.91\ and\ 0.83$) in predicting the normalised load–carrying capacity (see Table 2). It can be seen from the above discussion that the column slenderness has the same effect of the load eccentricity on the column Behaviour.

4.3 Effect of Longitudinal Reinforcement

The contribution of longitudinal reinforcement to normalised load-carrying capacity is highly dependent on the bending moment significance. If the neutral axis is located inside the column cross-section, revealing dominant bending moment, the column load-carrying capacity is improved by increasing longitudinal reinforcement content particularly in the tension side. These bars increase the tension stiffening effect and the flexure rigidity, subsequently enhancing the column stability. If entire cross-section is in compression, the increase in the normalised load-carrying capacity due to increasing the longitudinal reinforcement ratio is expected to be insignificant. Lee and Son (2000) reported that an increase of longitudinal steel ratio led to a larger increment of P/P_o value for a slender column than for a short column, and a more stable column. Moreover, the effect of longitudinal steel ratio was increased with the increase in concrete strength. Therefore, the increase of longitudinal reinforcement is more effective in slender HSC columns than that in short NSC columns. Kottb et al. (2015) reported that longitudinal steel ratio is one of the most effective factors influencing the ultimate load carrying capacity of high strength concrete columns. Figure 11 shows the longitudinal reinforcement effect on the column normalised load-carrying capacity confirming that increasing the reinforcement ratio resulted in an increase in the normalised load-carrying capacity. The prediction of normalised load-carrying capacity using NLFEA was improved as the reinforcement ratio increases. Table 4 indicates the enhancement in the normalised load-carrying capacity due to increasing longitudinal reinforcement ratio from 2.2% to 5.6% for columns of concrete compressive strengths of 70.4 and 93.2 MPa, eccentricity ratio of 0.17 to 0.54, and slenderness ratio of 19 to 61, respectively.

It can be seen from Table 4 and Figure 11 that the experimental results of Lee and Son (2000) indicate the existence of a proportional relationship between the concrete compressive strength and longitudinal reinforcement enhancement of load carrying capacity. Comparing the two pairs of Columns (HS1, HS1A) and (VS1, VS1A), indicates that increasing the concrete compressive strength from 70.4 MPa to 93.2 MPa resulted in increasing the enhancement of the load carrying capacity from 5.12% to 10.65%, respectively. The NLFEA predictions have the same trend as the analytical method (Abdel Karim et al., 2017) with enhancements ratios of (9.63% to 21.10%) and (9.18 to 19.94), respectively. As the eccentricity ratio increases, the enhancement becomes more significant because of the role of longitudinal reinforcement in increasing the tension stiffening effect. Increasing the eccentricity ratio from 0.21 to 0.54 resulted in an increase in the enhancement of the longitudinal reinforcement from (5.12 to 51.13), (9.63 to 53.73), and (9.18 to 63.8) for the results of experimental tests (Lee and Son, 2000), analytical method (Abdel Karim et al., 2017) and NLFEA developed model, respectively. Increasing the slenderness ratio had less effect than increasing eccentricity. Increasing slenderness ratio from 19 to 40 for columns of concrete compressive strength equals 93.2 MPa resulted in an increase in the enhancement from (11.33 to 27.87), (44.95 to 52.4), and (27.10 to 27.76) for the experimental results, analytical results and NLFEA results, respectively. It can be noticed from Table 4 that the

developed NLFEA model has the same sensitivity to the effect of longitudinal reinforcement as the analytical method (Abdel Karim et al., 2017) of the normalised load-carrying capacity.

5. Parametric Study to Compare NLFEA with Building Design Codes

5.1 Codes Provisions

A parametric study was carried out on additional 72 specimens using the provisions set by ECP-203, BS EN 1992-1-1:2004 Eurocode 2, and ACI-318-14 design Codes on the eccentric capacity to investigate the suitability of these design codes, which were originally used for the design of NSC columns, for the analysis and design of HSC slender/eccentric columns. The results are discussed through comparisons with the NLFEA results. The main difference between the codes procedure for predicting the load-carrying capacity of eccentric columns is the concept adopted to estimate the second-order bending moment acting on the critical cross-section. BS EN 1992-1-1:2004 Eurocode 2 (Eurocode 2) specifies two simplified methods to get the second-order bending moment to estimate the slender column load-carrying capacity, namely Eurocode 2-1 and Eurocode 2-2. These two methods are based on assessing either the nominal stiffness or the nominal curvature of the column. The NLFEA developed model was applied to the 70 column specimens of cross section (350 x 350) mm with concrete compressive strength of 100 MPa. A practical percentage of longitudinal reinforcement of 1.7 %, or 3.2 % with 400 MPa yield strength was considered. Two column specimens were selected to be examined on the effectiveness of confinement index(f_{ie}/f'_c), Column Type A had a confinement index of 0.03% and Column Type B had a confinement index of 5.14%. The shape of transverse reinforcement of each type is shown in Figure 12. It is worth mentioning that the effect of creep was not taken into account in the NLFEA. The two column specimens were used to generate the parametric study of eccentric columns with a load eccentricity ratio (e/h) ranging from 5% to 500% and slenderness ratio (λ) ranging from 25 to 200. The designation of columns starts with slenderness ratio, then by column Type A or B, and then by eccentricity ratio as shown in Figure 12 and indicated in Table 5. Figure 13 and Table 5 show that the load-carrying capacities predicted by ACI-318-14 Code are superior to other codes where the average of predictions was 0.99 with a coefficient of variation of 15%. ECP-203 Code predicts the load-carrying capacity by an average of 0.90 and 43% coefficient of variation. Whereas the two procedures specified by Eurocode 2 Code under-estimate the load-carrying capacity by an average of 0.63 and 0.67, and coefficient of variation of 25% and 33%, respectively. The observed under-estimation by Eurocode 2 Code increases as the slenderness ratio increases. This may be attributed to the confinement index taken into consideration in NLFEA was not consistent (ranged between 0.03% and 5.14%).

The results presented in Table 5 and Figure 14 show that overestimation of the column mid-height deformation yields in under-estimation of the load-carrying capacity. Consequently, the predicted mid-height deformation is the key aspect in assessing the column load-carrying capacity. It can be noticed that ACI-318-14 Code is better than the other codes in predicting mid-height deformation by an average of 1.28. In general, the methods of analysis may be classified into two main procedures as specified by Eurocode 2: nominal stiffness procedure, and nominal curvature procedure. The first category includes NLFEA, ACI-318-14 method, and Eurocode 2-1 method, while the second one includes the ECP-203 method, and Eurocode 2-2 method. Figure 14 shows that the results of the mid-height deflection predicted by the methods based on nominal curvature procedure are affected mainly by the slenderness ratio and overlook the effect of axial load level. On the other hand, the methods based on nominal stiffness take into consideration the axial load level and the slenderness ratio. The Eurocode

Accepted manuscript doi:
10.1680/jstbu.19.00064

2-1 method overestimates the mid-height deflection for all columns. Figure 15 and Table 5 illustrate the predicted enhancement in the load-carrying capacity by comparing the results of Column 'B' (with a confinement index of 5.14%) and Column 'A' (with a confinement index of 0.03%) for a wide range of e/h and slenderness ratios to study the effectiveness of confinement on eccentric columns. It can be seen from the figure that the confinement index has insignificant effect on the columns load-carrying capacity. Increasing confinement index of short columns with minimum eccentricity ratio resulted in an increase in the load-carrying capacity by approximately 3%. As the eccentricity or the slenderness ratio increases, no unified Behaviour is observed but the differences remain negligible. It can be noticed also from Table 5 that the studied design codes of practice do not consider the confinement parameters.

5.2 Load Eccentricity Ratio (e/h) & Slenderness Ratio (λ)

Figure 16 shows that increasing the load eccentricity lead to a reduction in the column load-carrying capacity and an increase in the mid-height deflection. It can be seen from the figure that the relation between the load eccentricity ratio and the column capacity either normalised by the cross-section capacity (Po) or the predicted ultimate load (P_{num}). Figure 17 shows the effect of slenderness ratio, λ, on the normalised load-carrying capacity of eccentrically loaded columns. It can be seen from the figure that when λ equals 25, ECP-203 Code is shown to overestimates the load-carrying capacity for columns with moderate eccentricity ratios of 0.2 and 0.4. The overestimation becomes more severe as λ increased to 50 and extended to columns with eccentricity ratio up to 1.00. This may be attributed neglecting the second-order deformation by ECP-203 Code for columns having a slenderness ratio ≤ 50. For a slenderness ratio ≥ 100, all codes under-estimated the column load-carrying capacity except ACI-318-14 Code which slightly overestimates load-carrying capacity of columns with eccentricity ratio ranging between 0.4 and 1.00. The design codes used in this investigation reflected the proportional relation between the slenderness ratio and the mid-height deformation. Increasing slenderness ratio lead to a reduction of the column load-carrying capacity. It can be seen from the figure that, up to slenderness ratio of 50, the load-carrying capacity results for columns having e/h ≤ 0.6 are scattered and ECP-203 overestimates column capacity. The studied design codes, except ACI-318-14, under-estimate the load-carrying capacity with increasing the slenderness ratio beyond 50. The ACI-318-14 Code slightly overestimates the load-carrying capacity for columns having an eccentricity ratio ranging between 0.4 and 1.00. The studied design codes under-estimate the load-carrying capacity for eccentricity ratio of 5.00.

Figure 18 shows the relation between the slenderness ratio, λ, and mid-height deflection, □, at wide range of loading eccentricity e/h. It can be seen from the figure that overestimation of the mid-height deflection as estimated by Eurocode 2-1 becomes more significant as the eccentricity ratio increased. On the other hand, the ACI-318-14 Code under-estimates the mid-height deflection as the eccentricity ratio increased. This trend illustrates that the normalised load-carrying capacity is dependent mainly on the prediction of column mid-height deflection. The mid-height deflection as predicted by Eurocode 2-2 method is shown to be constant for the range of eccentricity ratios investigated like ECP-203 Code. Second order effects may be ignored in Eurocode 2-2 if the slenderness ($\lambda = l_0/i$) is below a certain value λ_{lim}. The recommended value for the slenderness λ_{lim} was reported 75 elsewhere (BS EN 1992-1-1:2004 Eurocode 2). The stress-strain curve utilised by studied codes is another factor which should be considered in comparing the results. The ACI-318-14 code and ECP-203 code utilised stress-strain curves which are not applicable to HSC columns. This may

explain the overestimation in normalised load-carrying capacity for columns having eccentricity ratio of 0.4 and 0.6 predicted by ACI-318-14. However, the prediction of mid-height deflection by ACI-318-14 Code is comparable to that predicted by the NLFEA. The relationships between the predicted stiffness and the slenderness ratio are shown in Figure 19 to justify the difference between the methods of analysis in predicting results followed the nominal stiffness procedures. It can be seen from the figure that the main parameter that controls the mid-height deflection is the flexure stiffness. In addition, the Eurocode 2-1 procedure under-estimates the flexure stiffness for columns while the ACI-318-14 procedure slightly overestimates the flexure stiffness for columns having eccentricity ratio ≥ 0.8. It was noticed also that under-estimation of Eurocode 2-1 increases as the slenderness ratio increases.

6. Conclusions

A NLFEA model was developed to predict the behaviour of HSC columns subjected to eccentric loading. The model was verified by comparing the results with analytical and experimental results in the literature. In addition, parametric study was carried out to compare the prediction of HSC columns ‘strength analysis with the results obtained by the building design codes (ECP-203, ACI-318-14 and BS EN 1992) to assess the applicability of these codes for the design of HSC slender columns. The following conclusions are drawn from the study:

1. NLFEA developed model proved to be a suitable tool for predicting ultimate capacity and the strength analysis of slender HSC columns. Generally, an appreciable agreement was found between the predicted results and experimental column load-carrying capacity.
2. The ultimate load capacity of the columns reduced as the eccentricity of the applied load increases. Column slenderness was found to have the same effect as that of the load eccentricity. Increasing slenderness ratio lead to a reduction of ultimate load capacity. Prediction of column capacity enhancement was found higher than that of the experimental results, with the increase of longitudinal reinforcement, due to the tension-stiffening effect considered by the NLFEA developed model.
3. For a column entirely in compression, increasing longitudinal reinforcement has insignificant effect on the load-carrying capacity of the column. The enhancement of column capacity with longitudinal reinforcement was found proportional to concrete compressive strength, load eccentricity and slenderness ratio. Therefore, increasing longitudinal reinforcement to improve capacity is more effective in slender HSC columns than that for short and stable NSC columns.
4. ACI- 318-14 Code yielded the most conservative predictions of the load-carrying capacity of centric columns while the Eurocode 2 procedure based on nominal stiffness under-estimated the column flexure rigidity with increasing the slenderness or eccentricity ratio. The flexure rigidity estimated by ACI-318-14 increased with increasing the eccentricity ratio, particularly at low slenderness ratios.
5. The normalised load-carrying capacity of the columns predicted by NLFEA was reduced as the compressive strength of the concrete increases due to a consequential reduction in column confinement adopted in the NLFEA.
6. For eccentric columns, the predictions of ACI-318-14 code were well correlated with the NLFEA model predictions with a mean of 0.99 while the procedures (Eurocode 2-1 and

Eurocode 2-2) specified by BS EN 1992-1-1:2004 Eurocode 2, under-estimate the load-carrying capacity by an average of 0.63 and 0.67, and coefficient of variation of 25% and 33%, respectively. This under-estimation increases as the slenderness ratio increases and this is probably because the confinement index taken into consideration in the software was not consistent (ranged between 0.03% and 5.14%).

7. The ECP-203 code tends to overestimate the load-carrying capacity for columns having a slenderness ratio less than 50. For a slenderness ratio ≥ 100, all codes under-estimated the column load-carrying capacity except ACI-318-14 Code which slightly overestimates load-carrying capacity of columns with eccentricity ratio ranging between 0.4 and 1.00.
8. Based on the results of the current study, slender/eccentric HSC columns can be modeled accurately by the finite element approach using Ansys. In addition, among the available design codes, ACI 318-14 can be applied for the design of HSC slender columns while the other design codes need to provide special clauses for this purpose.

Notation

E_c is the concrete modulus of elasticity

E_s is the Young's Modulus of steel reinforcement

e/h load eccentricity ratio

f_c' is the unconfined concrete compressive strength

f_s and ε_s are the average stress and strain of the steel bars

f_y and ε_y are the yield stress and strain of steel bars

References

Abdel-Karim M (2016) Behaviour of Confined HSC Columns under Centric and Eccentric Loading. MSc thesis submitted to faculty of Engineering, Benha University, Cairo, Egypt, 181pp.

Abdel-Karim, M., Abdel-Rahman, G.T., Said, M and Shaaban, I.G.(2018). 'Proposed Model for Strength Analysis of HSC Eccentrically Loaded Slender Columns', Magazine of Concrete Research, Volume 70, Issue 7, pp. 340-349.
https://doi.org/10.1680/jmacr.17.00137

ACI Committee 318-14, 'Building code requirements for reinforced concrete (ACI 318-14) and commentary (ACI 318R-14),' American Concrete Institute, Farmington Hills, Mich.

Afefy, H. M. and El-Tony, M. E.-T. (2016) 'Simplified Design Procedure for Reinforced Concrete Columns Based on Equivalent Column Concept', International Journal of Concrete Structures and Materials. Korea Concrete Institute. doi: 10.1007/s40069-016-0132-0.

Angus, 2007, 'High-strength concrete columns: a design guide', the Structural Engineer, March 2007, pp. 31-38.

Ansys® (2009) 'Engineering Analysis System User's Manual, Vol. 1 & 2, and Theoretical Manual,' Revision 13.0, Swanson Analysis System Inc., Houston,Pennsylvania.

Attard, M M, and S Setunge (1996). 'Stress-Strain Relationship of Confined and Unconfined.' ACI Materials Journal 93, no. 5 (1996): 432-442.

Beal, A and Khalil, N. (1999). 'Design of normal- and high-strength concrete columns', Proc. Institution of Civil Engineering Structures & Buildings, Vol. 134, pp. 345 – 357, Paper 11847.

Brown, J. (2012). The Study of FRP Strengthening of Concrete Structures to Increase the Serviceable Design Life in Corrosive Environments., University of Western Australia, Perth, Australia, Research Report.

BS EN 1992-1-1:2004 Eurocode 2: Design of concrete structures. General rules and rules for buildings (incorporating corrigendum January 2008, November 2010 and February 2014)

Canbay, E., Ozcebe, G. and Ersoy, U. (2006) 'High-strength concrete columns under eccentric load', J. Struct. Eng., 132, pp. 1052–1060.

ECCS-203 (2017). 'Egyptian code for design and construction of reinforced concrete Structures,' Housing and Building Research Center, Egypt.

Foster, Stephen, J. and Attard, M. M. (1997). 'Experimental Tests on Eccentrically Loaded High-strength Concrete Columns.'', ACI Structural Journal, 94(3), pp. 295–303.

Galeota, D., Giammatteo, M. M. and Marino, R. (1992). 'Strength and Ductility of Confined High Strength', in Concrete Proceedings of 10th World Conference on Earthquake Engineering, Madrid, Spain, p. 2609–26 l 3.

Ghoneim, M. (2002). 'Strength of slender high-strength concrete columns under eccentric compression loads', Journal of Engineering and Applied Science, 49(6), pp. 1157–1176.

Habasaki, A., Kitada, Y., Nishikawa, T., Maekawa, K., UmekI, K., Yamada, M., and Kamimura, K., Feb. 2000, 'Shear Transfer Mechanism of Pr-Cracked RC Plates', No. 1493, 8 pp., Conference: 12th World Conference on Earthquake Engineering

Kim, J. and Yang, J. (1995). 'Buckling behaviour of slender high-strength concrete columns', Engineering Structures, 17(1), pp. 39–51.

Kottb, H. A., El-shafey, N. F. and Torkey, A. A. (2015). 'Behaviour of high strength concrete columns under eccentric loads', HBRC Journal. Housing and Building National Research Center, 11(1), pp. 22–34. doi: 10.1016/j.hbrcj.2014.02.006.

Lee, J.-H. and Son, H.-S. (2000). 'Failure and Strength of High-Strength Concrete Columns Subjected to Eccentric Loads.' .', ACI Structural Journal, 97(1), pp. 75–85.

Légeron, F. and Paultre, P. (2003). 'Uniaxial confinement model normal- and high-strength concrete columns.', ASCE Journal of Structural Engineering, 129(2), pp. 241–252.

Li, X. et al. (2017). 'Axial strength of FRP-confined rectangular RC columns with different cross-sectional aspect ratios', Magazine of Concrete Research, http://dx.

Lloyd, N. and Rangan, B. (1996). 'Studies on high-strength concrete columns under eccentric compression.', ACI Structural Journal, 93(6), pp. 631–638.

Niu, H. (2015). 'Full-scale testing of high-strength RACFST columns subjected to axial compression', Magazine of Concrete Research, 67(5), pp. 257–270.

Niu, H. and Cao, W. (2015). 'Full-scale testing of high-strength RACFST columns subjected to axial compression', Magazine of Concrete Research http://dx.doi.org/10.1680/macr.14.00198., 67(5), pp. 257–270.

Soliman, A. E. S. (2011). 'Behaviour of long confined concrete column', Ain Shams Engineering Journal. Faculty of Engineering, Ain Shams University, 2(3–4), pp. 141–148. doi: 10.1016/j.asej.2011.09.003.

Sudheer Reddy, L., Ramana Rao, N.V, Gunneswara Rao, T.D. (2015). 'Finite Element Analysis of High Strength Concrete Beams In Shear - Without Web Reinforcement and With Fiber in Shear Predominent Regions' International Journal of Innovative Research in Science, Engineering and Technology (An ISO 3297: 2007 Certified Organization) Vol. 4, Issue 4, pp. 2475-2484.

Wu, H.L, Wang, Y.F., Yu, L., and Li, X. (2009). 'Experimental and Computational Studies on High-Strength Concrete Circular Columns Confined by Aramid Fiber-Reinforced Polymer Sheets', Journal of Composites for Construction, Vol 13, No. 2.

Yang, T., Chang, Y., and Chang, S.Y. (2013). 'Prediction of Bilinear Stress-Strain Curve of Thin Hard Coating by Nanoindentation Test and Finite Element Method', Proceedings of the World Congress on Engineering 2013 Vol III, WCE 2013, July 3 - 5, 2013, London, U.K.

Zhou, W. and Hong, H. (2001). 'Statistical analyses of strength of slender RC columns', ASCE Journal of Structural Engineering, 127(1), pp. 21–27.

Accepted manuscript doi:
10.1680/jstbu.19.00064

Table 1 Comparison of current NLFEA results with experimental results by Lloyd and Rangan (1996)

Column	*fc*' (MPa)	ρ_{st} (%)	*l/r*	*e/h*	Ultimate response (Experimental results)		NLFEA (numerical results)	
					P_{exp} (kN)	Δ_{exp} (mm)	$\frac{P_{num}}{P_{exp}}$	$\frac{\Delta_{num}}{\Delta_{exp}}$
A1	58.0	2.16	30	0.09	1476	8.3	0.75	0.44
B1				0.29	830	12.5	0.77	0.48
C1				0.37	660	13.2	0.79	0.54
A5	92.0			0.09	1704	6.2	0.89	0.41
B5				0.29	1018	9.7	0.86	0.48
C5				0.37	795	12.3	0.89	0.49
A3	58.0	1.44		0.09	1140	8.8	0.91	0.35
B3				0.29	723	12.9	0.82	0.49
C3				0.37	511	11.7	0.93	0.68
A7	92.0			0.09	1745	7.6	0.83	0.30
B7				0.29	905	11.1	0.92	0.44
C7				0.37	663	15.4	0.98	0.42
A9	97.2			0.09	1932	5.6	0.83	0.70
B9				0.29	970	10.7	0.89	0.46
C9				0.37	747	13.9	0.92	0.47
Average							0.86	0.48

Accepted manuscript doi:
10.1680/jstbu.19.00064

Table2 Comparison of current NLFEA results with experimental results by Lee and Son (2000)

Column	*fc*' (MPa)	ρ_{st} (%)	*l/r*	*e/h*	Ultimate response (Experimental results)		NLFEA (numerical results)	
					P_{exp} (kN)	Δ_{exp} (mm)	$\frac{P_{num}}{P_{exp}}$	$\frac{\Delta_{num}}{\Delta_{exp}}$
HS1	70.4	2.18	19	0.21	529	0.9	0.90	1.72
HS2		2.18	19	0.38	333	2.8	0.98	0.95
HS3		2.18	19	0.54	187	3.5	0.91	0.81
HM1		2.18	40	0.17	508	8.1	0.91	0.53
HM2		2.18	40	0.38	307	10.8	0.98	0.79
HM3		2.18	40	0.54	156	10.1	1.20	0.95
HL1		2.18	61	0.17	523	19.7	0.83	0.46
HL2		2.18	61	0.38	205	18.4	1.23	0.81
HL3		2.18	61	0.54	118	14.9	1.57	1.43
HS1A		5.59	19	0.21	669	1.3	0.94	1.27
HS3A		5.59	19	0.54	340	2.9	1.05	0.79
HM1A		5.59	40	0.17	631	6.5	1.03	0.80
HM3A		5.59	40	0.54	273	10.4	1.07	0.73
HL1A		5.59	61	0.17	488	18.5	1.10	0.51
HL3A		5.59	61	0.54	216	23.2	1.16	0.82
VS1	93.2	2.18	19	0.21	655	2.6	0.91	0.85
VS2		2.18	19	0.38	416	2.7	0.91	0.92
VM1		2.18	40	0.17	639	8.2	0.93	0.64
VM2		2.18	40	0.38	324	13.5	1.09	0.66
VS1A		5.59	19	0.21	831	2.3	0.98	0.75
VS2A		5.59	19	0.38	531	2.4	1.04	0.85
VM1A		5.59	40	0.17	796	10.5	1.00	0.47
VM2A		5.59	40	0.38	475	12	1.04	0.63
Average							1.03	0.83

Accepted manuscript doi:
10.1680/jstbu.19.00064

Table 3 Comparison of current NLFEA results with experimental results by Foster et al. (1997)

Column	fc' (MPa)	ρ_{st} (%)	l/r	e/h	Ultimate response (Experimental results)		NLFEA (numerical results)	
					P_{exp} (kN)	Δ_{exp} (mm)	$\frac{P_{num}}{P_{exp}}$	$\frac{\Delta_{num}}{\Delta_{exp}}$
2M8-30	75.0	2.04	15	0.05	1348	5	0.93	0.37
2M8-60	75.0	2.04	15	0.05	1432	5	0.82	0.30
2M8-120	75.0	2.04	15	0.05	1239	4	0.92	0.36
2M20-30	74.0	2.04	15	0.13	1160	6	0.90	0.60
2M20-60	74.0	2.04	15	0.13	1231	6	0.73	0.47
2M20-120	74.0	2.04	15	0.13	1067	5	0.84	0.55
2M50-30	74.0	2.04	15	0.33	630	9.5	1.06	0.65
2M50-60	74.0	2.04	15	0.33	670	8.4	0.86	0.72
2M50-120	74.0	2.04	15	0.33	652	11.5	0.83	0.46
4M8-30	74.0	4.09	15	0.05	1102	3	1.29	0.68
4M8-60	75.0	4.09	15	0.05	1404	4	0.94	0.40
4M8-120	74.0	4.09	15	0.05	1404	3.5	0.93	0.42
4M20-30	75.0	4.09	15	0.13	1052	4	1.17	0.94
4M20-60	75.0	4.09	15	0.13	1198	4.4	0.83	0.60
4M20-120	75.0	4.09	15	0.13	1105	7.2	0.89	0.38
4M50-30	74.0	4.09	15	0.33	656	9.5	1.13	0.62
4M50-60	75.0	4.09	15	0.33	686	9.5	0.99	0.63
4M50-120	74.0	4.09	15	0.33	633	9.5	1.03	0.55
2H8-30	93.0	2.04	15	0.05	1576	3.5	0.96	0.41
2H8-60	93.0	2.04	15	0.05	1647	4.5	0.88	0.37
2H8-120	93.0	2.04	15	0.05	1806	3.6	0.80	0.47
2H20-30	92.0	2.04	15	0.13	1207	6.5	0.97	0.50
2H20-60	92.0	2.04	15	0.13	1247	5.3	0.89	0.58
2H20-120	92.0	2.04	15	0.13	1473	5.6	0.75	0.55
2H50-30	92.0	2.04	15	0.33	749	9.7	0.95	0.58
2H50-60	92.0	2.04	15	0.33	685	10	0.96	0.51
2H50-120	92.0	2.04	15	0.33	851	8.3	0.76	0.59
4H8-30	91.0	4.09	15	0.05	1601	4.8	1.04	0.37
4H8-60	92.0	4.09	15	0.05	1702	5.5	0.95	0.31
4H8-120	92.0	4.09	15	0.05	1654	4.2	0.97	0.40
4H20-30	88.0	4.09	15	0.13	1352	7	1.06	0.63
4H20-60	88.0	4.09	15	0.13	1358	7.5	0.94	0.53
4H20-120	92.0	4.09	15	0.13	1374	7	0.89	0.45
4H50-30	88.0	4.09	15	0.33	780	10.5	1.00	0.51
4H50-60	88.0	4.09	15	0.33	790	9.5	0.96	0.53
4H50-120	92.0	4.09	15	0.33	818	9.5	0.91	0.59

Accepted manuscript doi:
10.1680/jstbu.19.00064

Column	*fc'* (MPa)	ρ_{st} (%)	*l/r*	*e/h*	Ultimate response (Experimental results)		NLFEA (numerical results)	
					P_{exp} (kN)	Δ_{exp} (mm)	$\frac{P_{num}}{P_{exp}}$	$\frac{\Delta_{num}}{\Delta_{exp}}$
Average							0.94	0.52

Table 4 Longitudinal reinforcement enhancement to the load-carrying capacity (prediction of specimens experimental tested by Lee and Son, 2000)

Column	f_c' *(MPa)*	λ	*e/h*	ρ_s (%)	P/P_o			Enhancement (%)		
					EXP	Analytical Model (Abdel-Karim et al, 2017)	NLFEA	EXP	Analytical Model (Abdel-Karim et al, 2017)	NLFEA
HS1	70.4	19	0.21	2.2	0.48	0.47	0.43	5.12	9.63	9.18
HS1A				5.6	0.50	0.51	0.47			
HM1		40	0.17	2.2	0.46	0.41	0.42	3.25	17.58	17.12
HM1A				5.6	0.47	0.48	0.49			
HL1		61	0.17	2.2	0.47	0.29	0.39	-22.44	17.81	2.23
HL1A				5.6	0.37	0.35	0.40			
HS3		19	0.54	2.2	0.17	0.17	0.16	51.13	53.73	63.80
HS3A				5.6	0.26	0.27	0.27			
HM3		40	0.54	2.2	0.14	0.14	0.16	45.46	64.17	37.13
HM3A				5.6	0.21	0.23	0.22			
HL3		61	0.54	2.2	0.11	0.11	0.15	52.16	58.63	26.20
HL3A				5.6	0.16	0.18	0.19			
VS1	93.2	19	0.21	2.2	0.46	0.44	0.42	10.65	21.10	19.94
VS1A				5.6	0.51	0.54	0.50			
VS2		19	0.38	2.2	0.29	0.26	0.26	11.33	44.95	27.10
VS2A				5.6	0.32	0.37	0.34			
VM1		40	0.17	2.2	0.45	0.39	0.42	8.65	20.77	16.39
VM1A				5.6	0.48	0.47	0.48			
VM2		40	0.38	2.2	0.23	0.19	0.25	27.87	52.40	27.76
VM2A				5.6	0.29	0.29	0.30			

Accepted manuscript doi:
10.1680/jstbu.19.00064

Table 5 Parametric Results of Eccentric Columns

Column Specimen	l / r	e / h	I_e	NLFEA (numerical results)		ECP-203		BS EN 1992-1-1:2004 Eurocode 2				ACI-318-14	
								EC2-1		EC2-2			
				P_{num} (kN)	Δ_{num} (mm)	$\frac{P}{P_{num}}$	$\frac{\Delta}{\Delta_{num}}$	$\frac{P}{P_{num}}$	$\frac{\Delta}{\Delta_{num}}$	$\frac{P}{P_{num}}$	$\frac{\Delta}{\Delta_{num}}$	$\frac{P}{P_{num}}$	$\frac{\Delta}{\Delta_{num}}$
25A5	25	0.05	0.03	8905.78	6.24	0.95	1.54	0.94	0.21	0.91	0.98	1.07	0.38
25B5	25	0.05	5.14	9059.18	5.80	0.92	1.74	0.91	0.24	0.88	1.11	1.05	0.43
25A20	25	0.20	0.03	4699.50	17.41	1.41	0.56	0.97	1.26	1.07	0.67	1.12	1.44
25B20	25	0.20	5.14	4662.74	20.38	1.49	0.49	1.03	1.12	1.13	0.60	1.19	1.28
25A40	25	0.40	0.03	2442.44	18.64	1.38	0.52	0.79	2.14	1.03	0.70	1.08	1.13
25B40	25	0.40	5.14	2409.96	19.48	1.37	0.49	0.79	2.03	1.03	0.67	1.09	1.07
25A60	25	0.60	0.03	1408.13	17.39	1.12	0.56	0.76	2.05	0.91	0.76	1.02	0.63
25B60	25	0.60	5.14	1381.91	17.43	1.16	0.56	0.79	2.08	0.95	0.77	1.06	0.64
25A80	25	0.80	0.03	911.92	15.43	0.93	0.60	0.74	2.20	0.83	0.81	0.89	0.43
25B80	25	0.80	5.14	897.67	14.97	0.89	0.58	0.70	2.13	0.79	0.79	0.86	0.41
25A100	25	1.00	0.03	655.61	14.17	0.85	0.62	0.71	2.29	0.77	0.85	0.83	0.35
25B100	25	1.00	5.14	648.51	14.69	0.89	0.62	0.73	2.29	0.81	0.84	0.87	0.34
25A500	25	5.00	0.03	89.53	12.56	0.83	0.71	0.80	3.10	0.80	0.97	0.79	0.22
25B500	25	5.00	5.14	90.59	8.05	0.77	1.04	0.74	4.54	0.74	1.42	0.73	0.31
50A5	50	0.05	0.03	7068.20	30.38	1.45	1.35	1.23	0.12	0.94	1.31	1.22	0.89
50B5	50	0.05	5.14	7213.01	33.27	1.40	1.21	1.18	0.11	0.91	1.18	1.18	0.80
50A20	50	0.20	0.03	3025.11	50.21	2.02	0.71	0.69	1.73	1.04	0.98	0.85	1.62
50B20	50	0.20	5.14	2945.61	57.18	2.05	0.62	0.70	1.50	1.05	0.85	0.86	1.41
50A40	50	0.40	0.03	1704.41	55.14	1.96	0.69	0.72	1.55	0.99	0.95	1.06	0.99
50B4	50	0.	5.	1662.88	55.48	2.0	0.7	0.74	1.55	1.01	0.95	1.0	0.9

Column Specimen	l / r	e / h	I_e	NLFEA (numerical results)		ECP-203		BS EN 1992-1-1:2004 Eurocode 2				ACI-318-14	
								EC2-1		EC2-2			
				P_{num} (kN)	Δ_{num} (mm)	$\frac{P}{P_{num}}$	$\frac{\Delta}{\Delta_{num}}$	$\frac{P}{P_{num}}$	$\frac{\Delta}{\Delta_{num}}$	$\frac{P}{P_{num}}$	$\frac{\Delta}{\Delta_{num}}$	$\frac{P}{P_{num}}$	$\frac{\Delta}{\Delta_{num}}$
0		40	14			2	0					9	8
50A60	50	0.60	0.03	1072.05	77.10	1.39	0.48	0.68	1.10	0.85	0.66	1.02	0.43
50B60	50	0.60	5.14	1052.44	52.99	1.43	0.70	0.70	1.60	0.87	0.95	1.04	0.63
50A80	50	0.80	0.03	753.52	74.30	1.15	0.50	0.68	1.19	0.82	0.68	0.98	0.33
50B80	50	0.80	5.14	745.73	45.48	0.07	0.05	0.04	0.11	0.05	0.06	0.06	0.03
50A100	50	1.00	0.03	570.26	71.12	1.01	0.51	0.68	1.29	0.79	0.70	0.91	0.27
50B100	50	1.00	5.14	565.13	41.55	1.04	0.90	0.69	2.26	0.81	1.22	0.94	0.47
50A500	50	5.00	0.03	88.83	67.53	0.87	0.54	0.76	2.06	0.81	0.74	0.82	0.17
50B500	50	5.00	5.14	89.27	30.54	0.89	1.25	0.79	4.71	0.83	1.71	0.85	0.39
100A5	100	0.05	0.03	3076.76	45.79	0.71	3.27	0.49	3.84	0.38	4.46	0.50	4.23
100B5	100	0.05	5.14	3057.37	39.40	0.73	3.82	0.50	4.48	0.38	5.20	0.51	4.93
100A20	100	0.20	0.03	1392.12	156.80	0.93	0.95	0.70	1.12	0.59	1.30	0.91	0.98
100B20	100	0.20	5.14	1375.03	116.67	0.95	1.30	0.71	1.53	0.60	1.77	0.93	1.33
100A40	100	0.40	0.03	895.72	138.92	0.89	1.09	0.66	1.41	0.63	1.50	1.10	0.89
100B40	100	0.40	5.14	884.86	127.35	0.90	1.20	0.68	1.55	0.65	1.64	1.11	0.97
100A60	100	0.60	0.03	652.92	128.99	0.86	1.20	0.64	1.74	0.67	1.63	1.14	0.79
100B60	100	0.60	5.14	640.18	120.12	0.87	1.27	0.65	1.85	0.68	1.74	1.16	0.84
100A80	100	0.80	0.03	507.60	195.41	0.89	0.82	0.64	1.32	0.72	1.12	1.15	0.45
100B80	100	0.80	5.14	502.50	118.48	0.89	1.34	0.65	2.16	0.73	1.83	1.16	0.73
100A100	100	1.00	0.03	414.72	191.35	0.89	0.85	0.66	1.50	0.75	1.16	1.14	0.41
100B100	100	1.00	5.14	411.54	130.68	0.88	1.24	0.65	2.16	0.75	1.68	1.12	0.58

Column Specimen	l / r	e / h	I_e	NLFEA (numerical results)		ECP-203		BS EN 1992-1-1:2004 Eurocode 2				ACI-318-14	
								EC2-1		EC2-2			
				P_{num} (kN)	Δ_{num} (mm)	$\frac{P}{P_{num}}$	$\frac{\Delta}{\Delta_{num}}$	$\frac{P}{P_{num}}$	$\frac{\Delta}{\Delta_{num}}$	$\frac{P}{P_{num}}$	$\frac{\Delta}{\Delta_{num}}$	$\frac{P}{P_{num}}$	$\frac{\Delta}{\Delta_{num}}$
100A500	100	5.00	0.03	84.17	244.18	0.76	0.56	0.62	1.73	0.72	0.76	0.80	0.17
100B500	100	5.00	5.14	84.52	126.05	0.75	1.08	0.62	3.35	0.71	1.47	0.79	0.34
150A5	150	0.05	0.03	1440.98	42.44	0.33	7.21	0.44	5.97	0.21	9.82	0.55	5.26
150B5	150	0.05	5.14	1424.65	42.57	0.34	7.19	0.45	5.96	0.22	9.81	0.56	5.25
150A20	150	0.20	0.03	767.67	185.60	0.52	1.65	0.54	1.55	0.35	2.24	0.89	1.09
150B20	150	0.20	5.14	746.72	187.53	0.55	1.65	0.56	1.56	0.36	2.26	0.92	1.08
150A40	150	0.40	0.03	555.79	166.77	0.60	1.92	0.53	2.16	0.42	2.63	1.04	1.10
150B40	150	0.40	5.14	541.66	167.45	0.62	1.93	0.54	2.17	0.45	2.62	1.07	1.11
150A60	150	0.60	0.03	434.30	212.06	0.70	1.66	0.56	2.14	0.53	2.27	1.19	0.84
150B60	150	0.60	5.14	425.34	218.66	0.68	1.50	0.53	1.94	0.50	2.05	1.13	0.77
150A80	150	0.80	0.03	359.63	206.35	0.75	1.74	0.56	2.50	0.58	2.36	1.20	0.81
150B80	150	0.80	5.14	353.96	215.07	0.75	1.65	0.56	2.37	0.58	2.25	1.21	0.77
150A100	150	1.00	0.03	306.81	218.31	0.71	1.51	0.50	2.36	0.56	2.06	1.09	0.66
150B100	150	1.00	5.14	302.27	207.92	0.78	1.72	0.56	2.69	0.62	2.35	1.20	0.75
150A500	150	5.00	0.03	78.75	253.75	0.78	1.22	0.55	3.40	0.67	1.66	0.84	0.38
150B500	150	5.00	5.14	78.06	284.36	0.79	1.09	0.55	3.03	0.68	1.48	0.85	0.34
200A5	200	0.05	0.03	801.62	40.80	0.30	14.15	0.34	12.28	0.20	18.64	0.67	8.16
200B5	200	0.05	5.14	796.74	40.96	0.29	14.02	0.34	12.17	0.21	18.48	0.67	8.10
200A20	200	0.20	0.03	481.47	266.36	0.50	2.40	0.46	2.46	0.35	3.16	1.09	1.21
200B20	200	0.20	5.14	468.57	265.95	0.51	2.41	0.48	2.47	0.36	3.17	1.12	1.22
200A	20	0.	0.	380.22	258.82	0.5	2.4	0.45	3.00	0.41	3.27	1.1	1.1

Column Specimen	l / r	e / h	I_e	NLFEA (numerical results)		ECP-203		BS EN 1992-1-1:2004 Eurocode 2				ACI-318-14	
								EC2-1		EC2-2			
				P_{num} (kN)	Δ_{num} (mm)	$\frac{P}{P_{num}}$	$\frac{\Delta}{\Delta_{num}}$	$\frac{P}{P_{num}}$	$\frac{\Delta}{\Delta_{num}}$	$\frac{P}{P_{num}}$	$\frac{\Delta}{\Delta_{num}}$	$\frac{P}{P_{num}}$	$\frac{\Delta}{\Delta_{num}}$
40	0	40	03			6	8					8	6
200B 40	200	0.40	5.14	371.54	259.49	0.58	2.50	0.46	3.01	0.42	3.29	1.21	1.17
200A 60	200	0.60	0.03	312.88	252.02	0.59	2.49	0.44	3.37	0.45	3.29	1.19	1.11
200B 60	200	0.60	5.14	299.67	348.73	0.66	1.90	0.48	2.56	0.49	2.50	1.31	0.84
200A 80	200	0.80	0.03	269.44	257.45	0.72	2.78	0.51	4.13	0.56	3.67	1.36	1.17
200B 80	200	0.80	5.14	259.07	329.89	0.66	1.92	0.46	2.84	0.50	2.53	1.25	0.80
200A 100	200	1.00	0.03	232.97	342.75	0.71	1.95	0.48	3.09	0.55	2.56	1.29	0.78
200B 100	200	1.00	5.14	230.12	258.49	0.71	2.54	0.48	4.03	0.55	3.34	1.28	1.02
200A 500	200	5.00	0.03	71.04	405.72	0.84	1.38	0.49	3.61	0.75	1.76	0.90	0.44
200B 500	200	5.00	5.14	70.45	463.96	0.84	1.21	0.49	3.14	0.76	1.53	0.90	0.37
Average						0.90	1.84	0.63	2.58	0.67	2.42	0.99	1.20

Accepted manuscript doi:
10.1680/jstbu.19.00064

Figure captions

Figure 1 Typical idealization of HSC columns (a) Concrete element; Solid 65, (b) Reinforcing bar element; 3D-Link 180

Figure 2 Attard and Setunge (1996) Stress-Strain Relationship

Figure 3 Bilinear stress-strain idealization for steel reinforcement (Yang et al., 2013)

Figure 4 Applied boundary conditions in the model

Figure 5 Load-deflection prediction at mid-height for columns experimentally tested by Lloyd and Rangan (1996) (a) Columns have a concrete compressive strength of 58MPa, (b) Columns have a concrete compressive strength of 97MPa

Figure 6 Correlation between the experimental and predicted results using NLFEA (a) Mid-height deflection in (mm), (b) Normalized load-carrying capacity

Figure 7 NLFEA prediction of Column HM3 tested by Lee and Son (2000) (a) Cracks propagation, (b) Stresses contour plots

Figure 8 Concrete Strength effect on the column normalized load-carrying capacity (a) loading eccentricity (experimentally tested by Lloyd and Rangan, 1996), (b) Slenderness ratio (experimentally tested by Lee and Son, 2000), (c) Reinforcement ratio and configuration (experimentally tested by Foster et al., 1997)

Figure 9 Eccentricity ratio effect on the column normalized load-carrying capacity (a) Concrete strength (experimentally tested by Lloyd and Rangan, 1996), (b) Tie spacing (experimentally tested by Foster et al., 1997), (c) Slenderness ratio (experimentally tested by Lee and Son, 2000)

Figure 10 Slenderness ratio effect on the column normalized load-carrying capacity (experimentally tested by Lee and Son, 2000) (a) Load eccentricity, (b) Longitudinal reinforcement ratio and/or concrete compressive strength

Figure 11 Longitudinal reinforcement ratio effect on the column normalized load-carrying capacity (Column specimens experimentally tested by Lee and Son, 2000)

Accepted manuscript doi:
10.1680/jstbu.19.00064

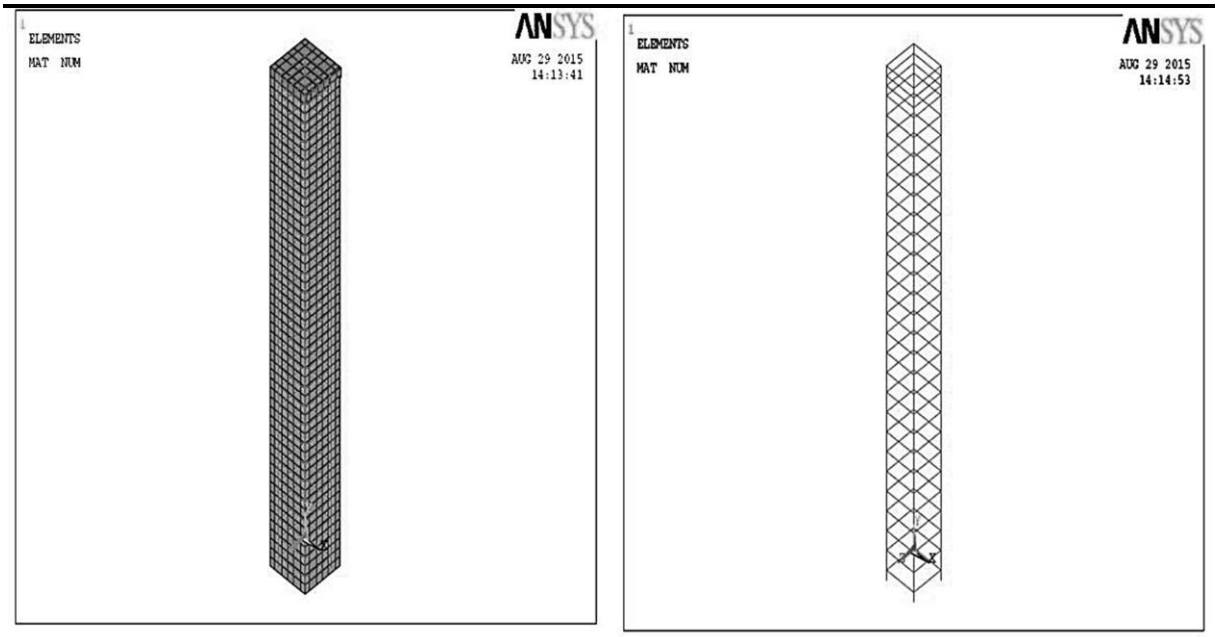

a) Concrete element; Solid 65 b) Reinforcing bar element; 3D-Link 180

Figure 1

Accepted manuscript doi:
10.1680/jstbu.19.00064

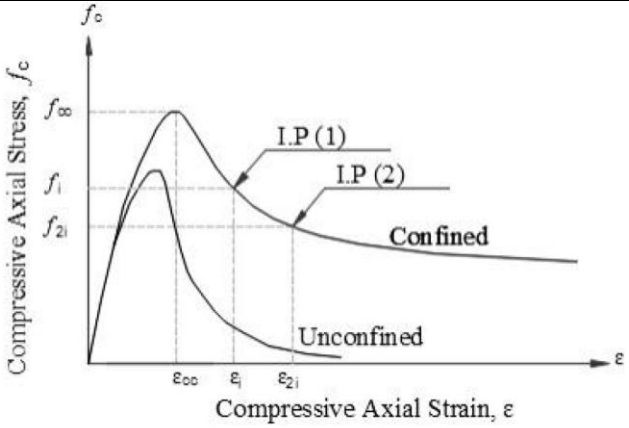

Figure 2

Accepted manuscript doi:
10.1680/jstbu.19.00064

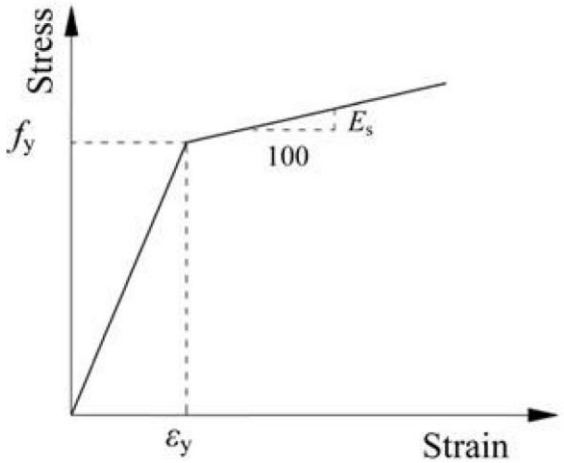

Figure 3

Accepted manuscript doi:
10.1680/jstbu.19.00064

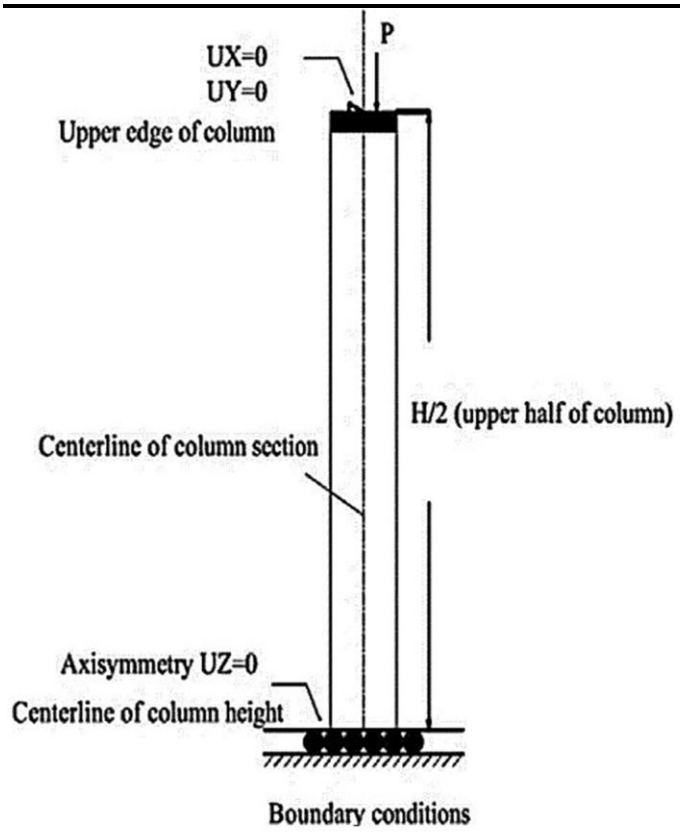

Figure 4

Accepted manuscript doi:
10.1680/jstbu.19.00064

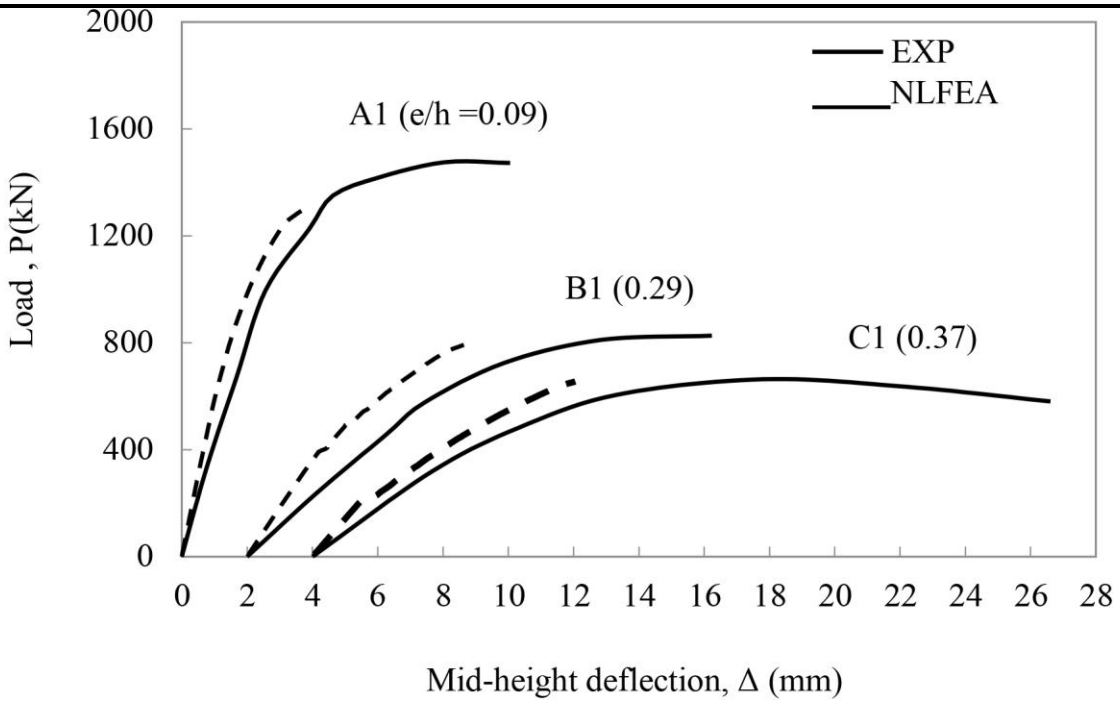

a) Columns have a concrete compressive strength of 58MPa

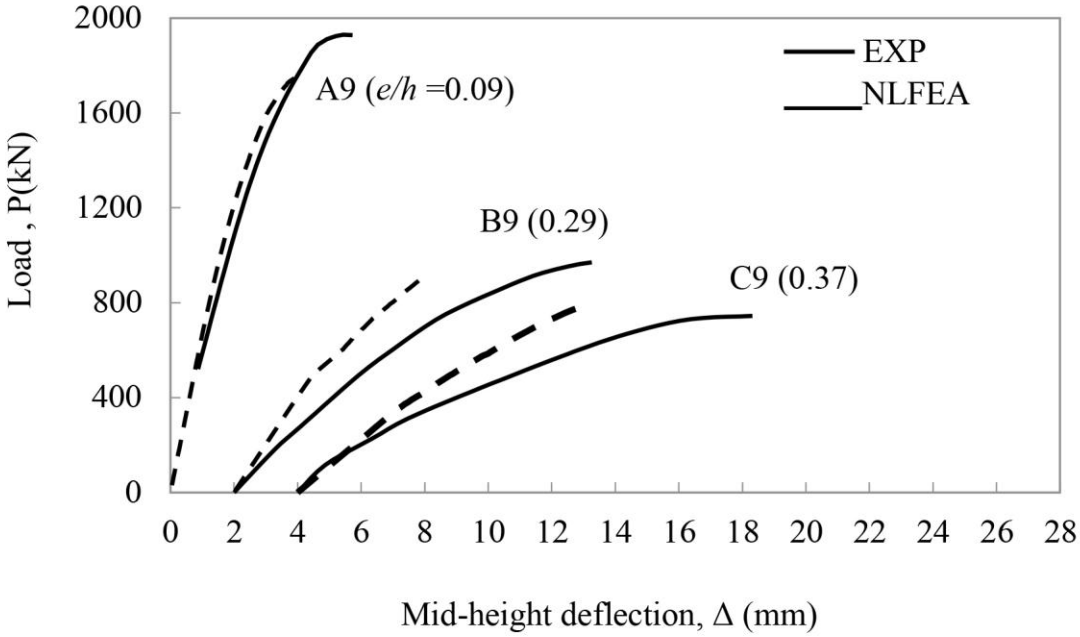

b) Columns have a concrete compressive strength of 97MPa

Figure 5

Accepted manuscript doi:
10.1680/jstbu.19.00064

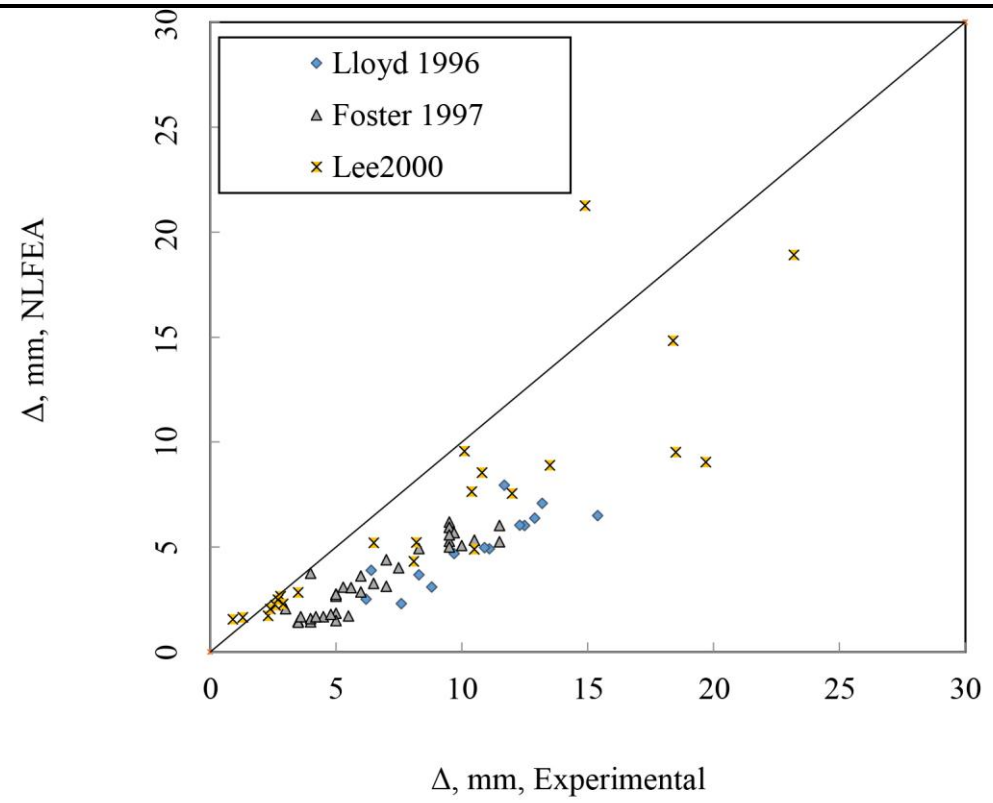

(a) Mid-height deflection in (mm)

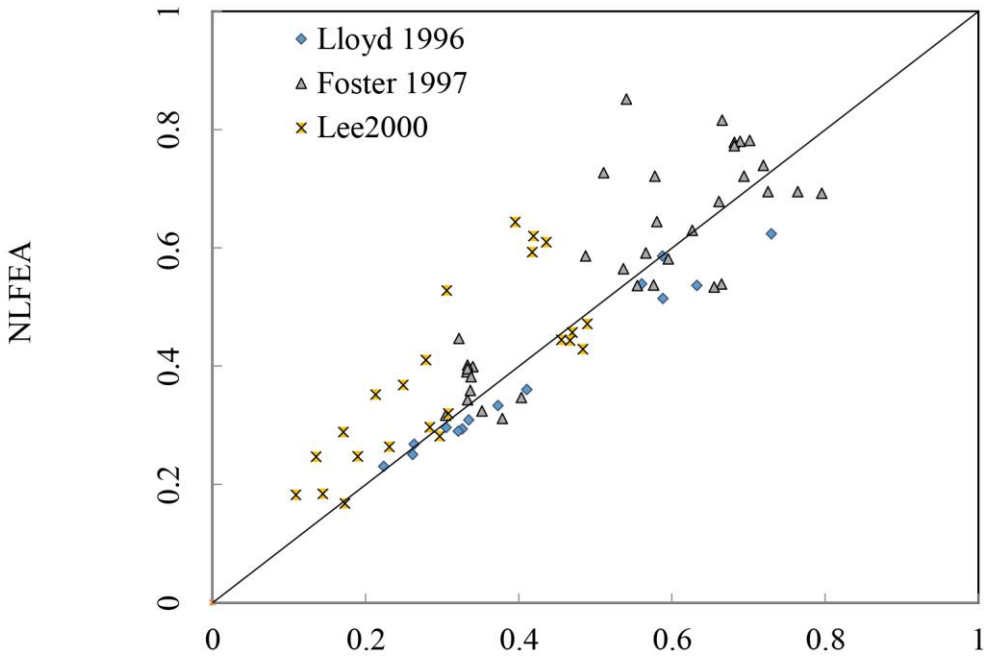

(b) Normalized load-carrying capacity

Figure 6

Accepted manuscript doi:
10.1680/jstbu.19.00064

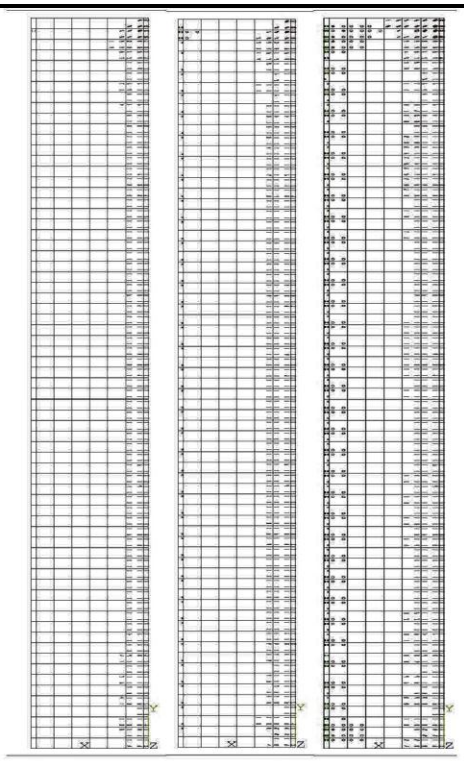

(a) Cracks propagation

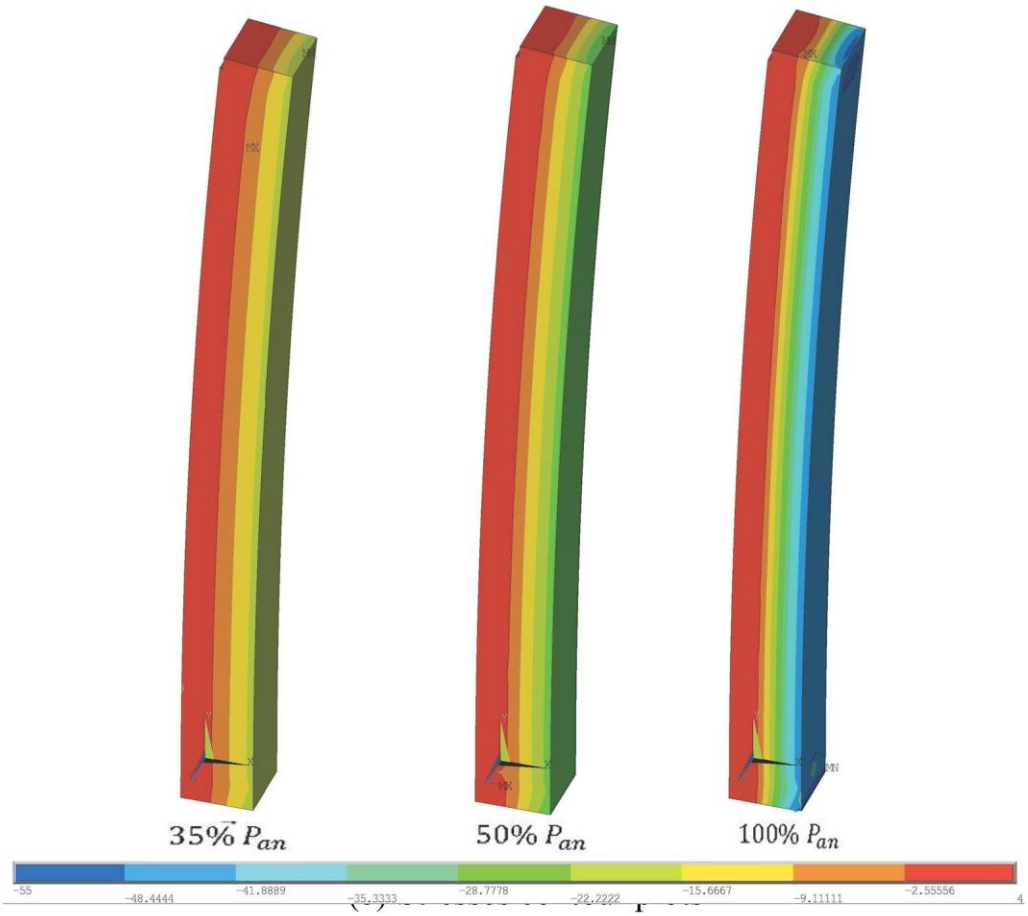

Figure 7

Accepted manuscript doi:
10.1680/jstbu.19.00064

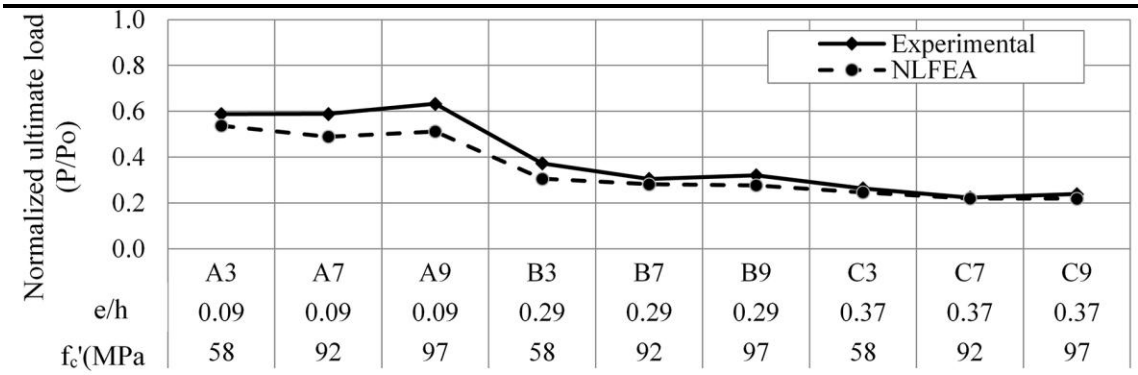

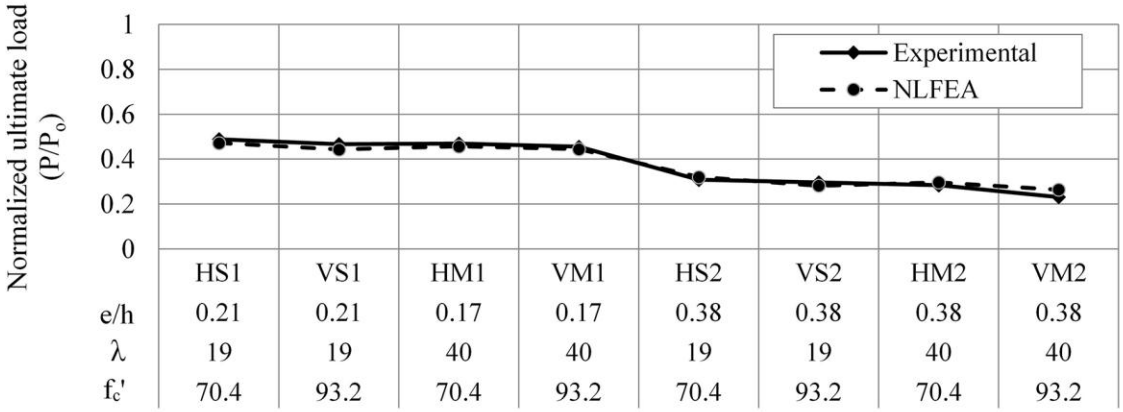

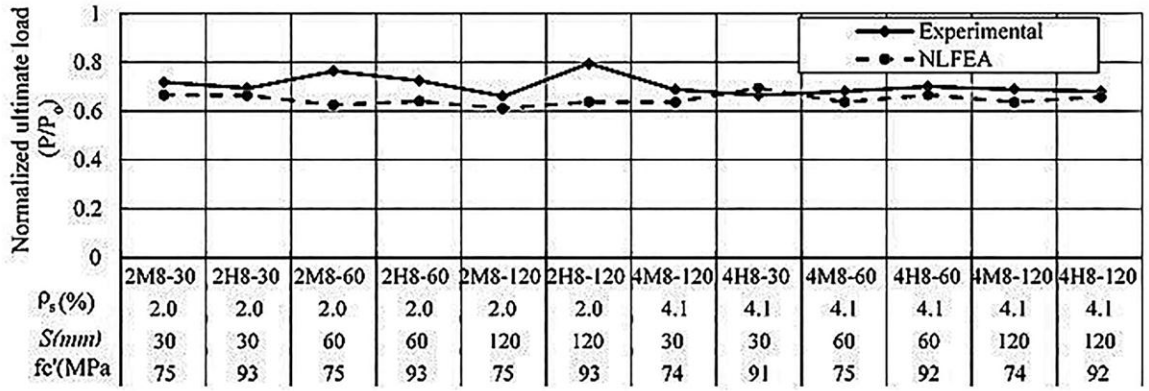

Figure 8

Accepted manuscript doi:
10.1680/jstbu.19.00064

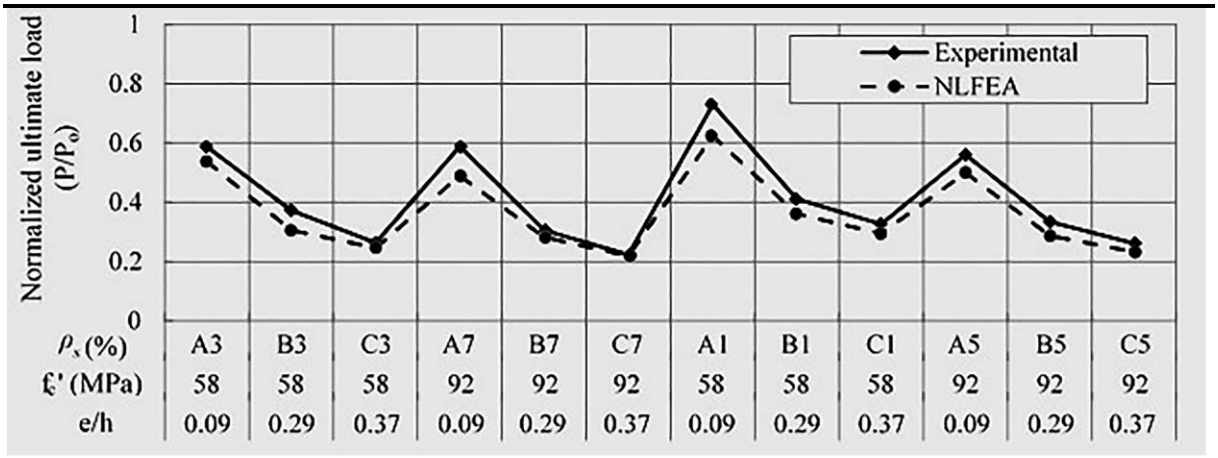

a) Concrete strength (experimentally tested by Lloyd and Rangan, 1996)

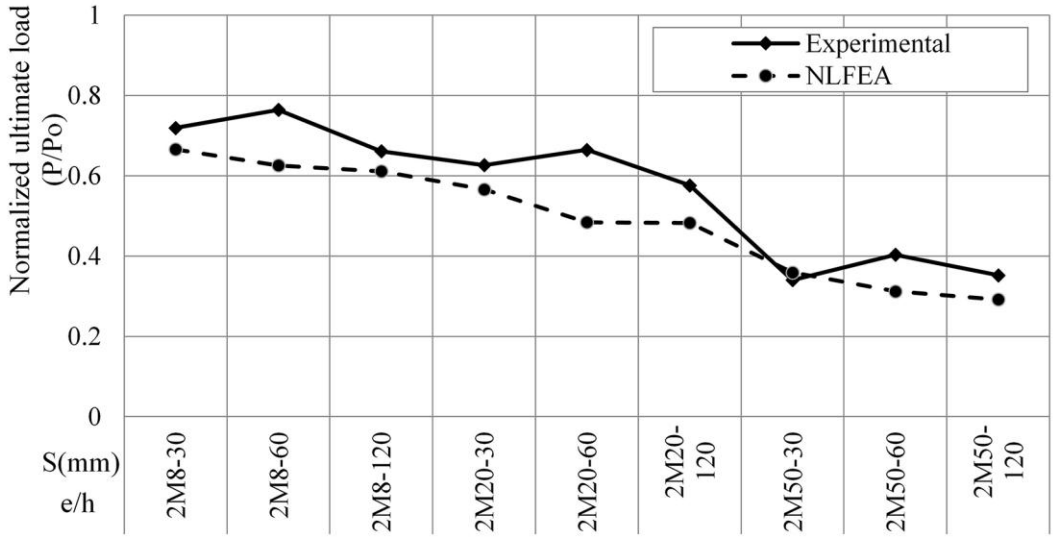

b) Tie spacing (experimentally tested by Foster et al., 1997)

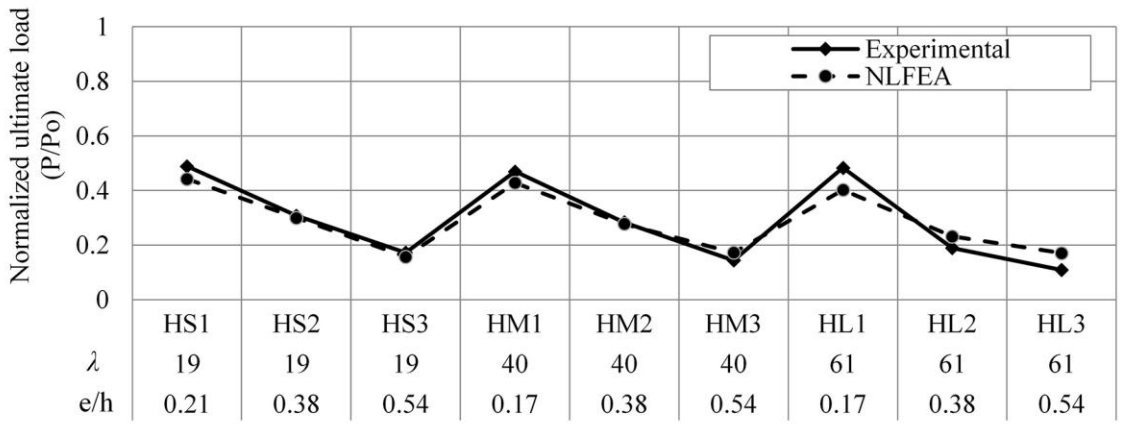

c) Slenderness ratio (experimentally tested by Lee and Son, 2000)

Figure 9

Accepted manuscript doi:
10.1680/jstbu.19.00064

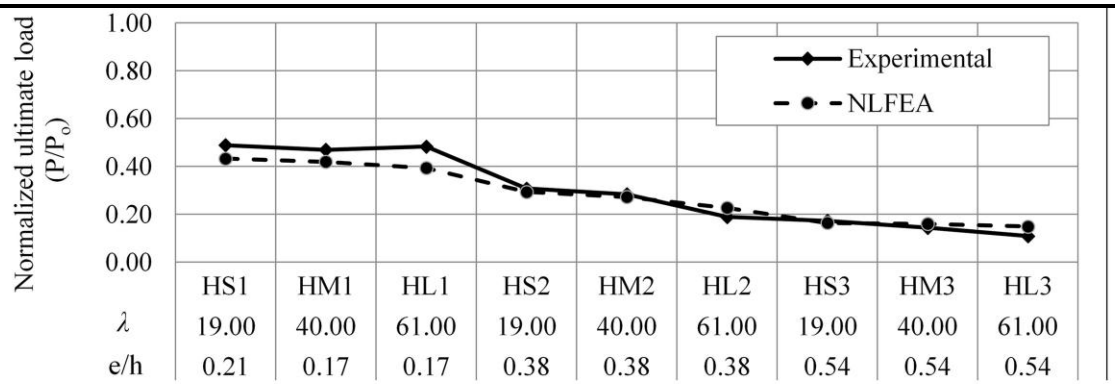

a) Load eccentricity

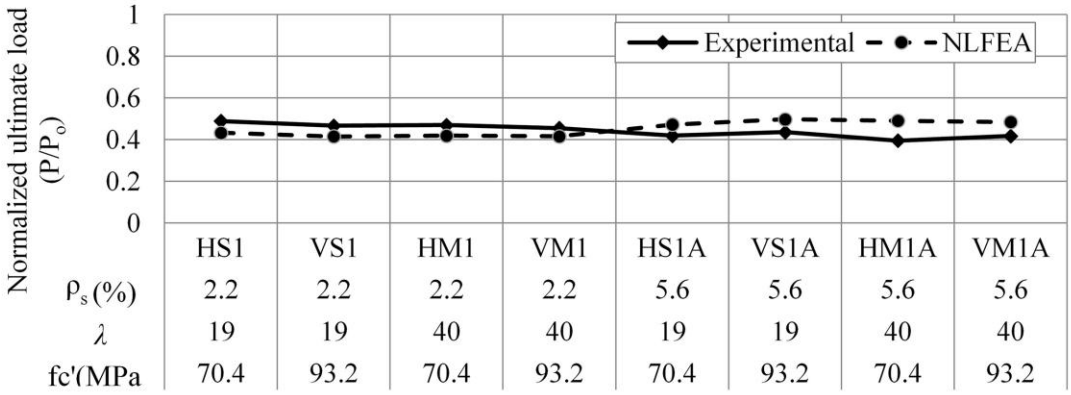

b) Longitudinal reinforcement ratio and/or concrete compressive strength

Figure 10

Accepted manuscript doi:
10.1680/jstbu.19.00064

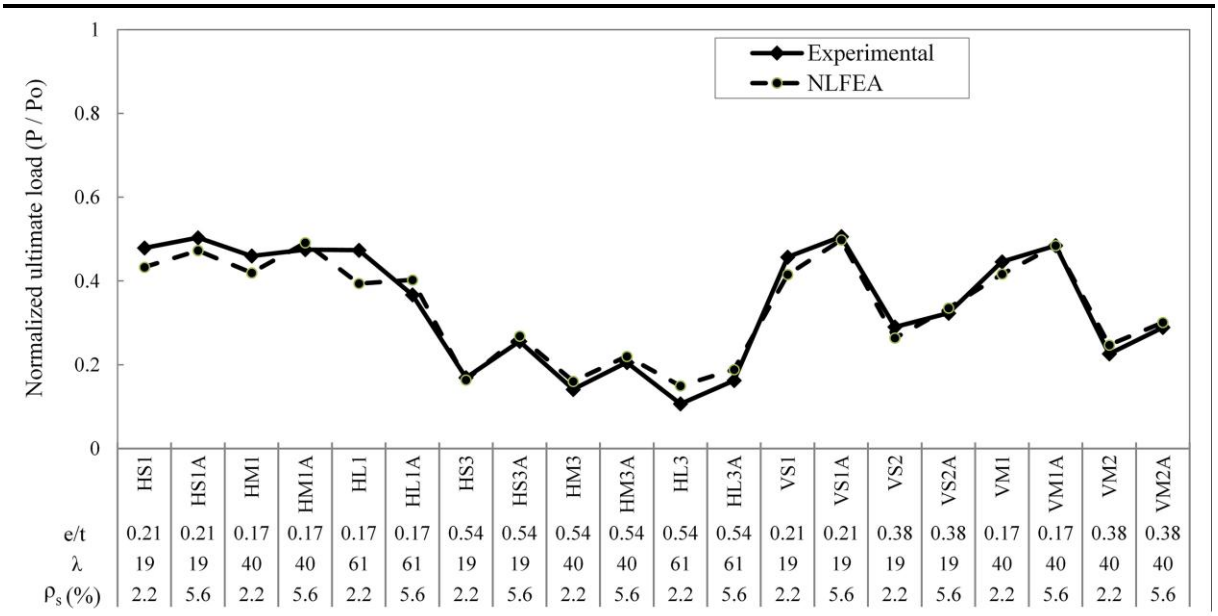

Figure 11

Accepted manuscript doi:
10.1680/jstbu.19.00064

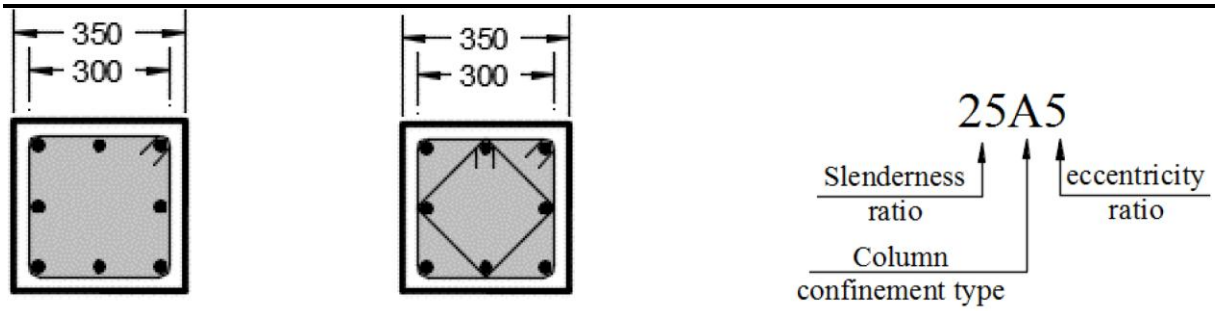

Type A Type B

Figure 12

Accepted manuscript doi:
10.1680/jstbu.19.00064

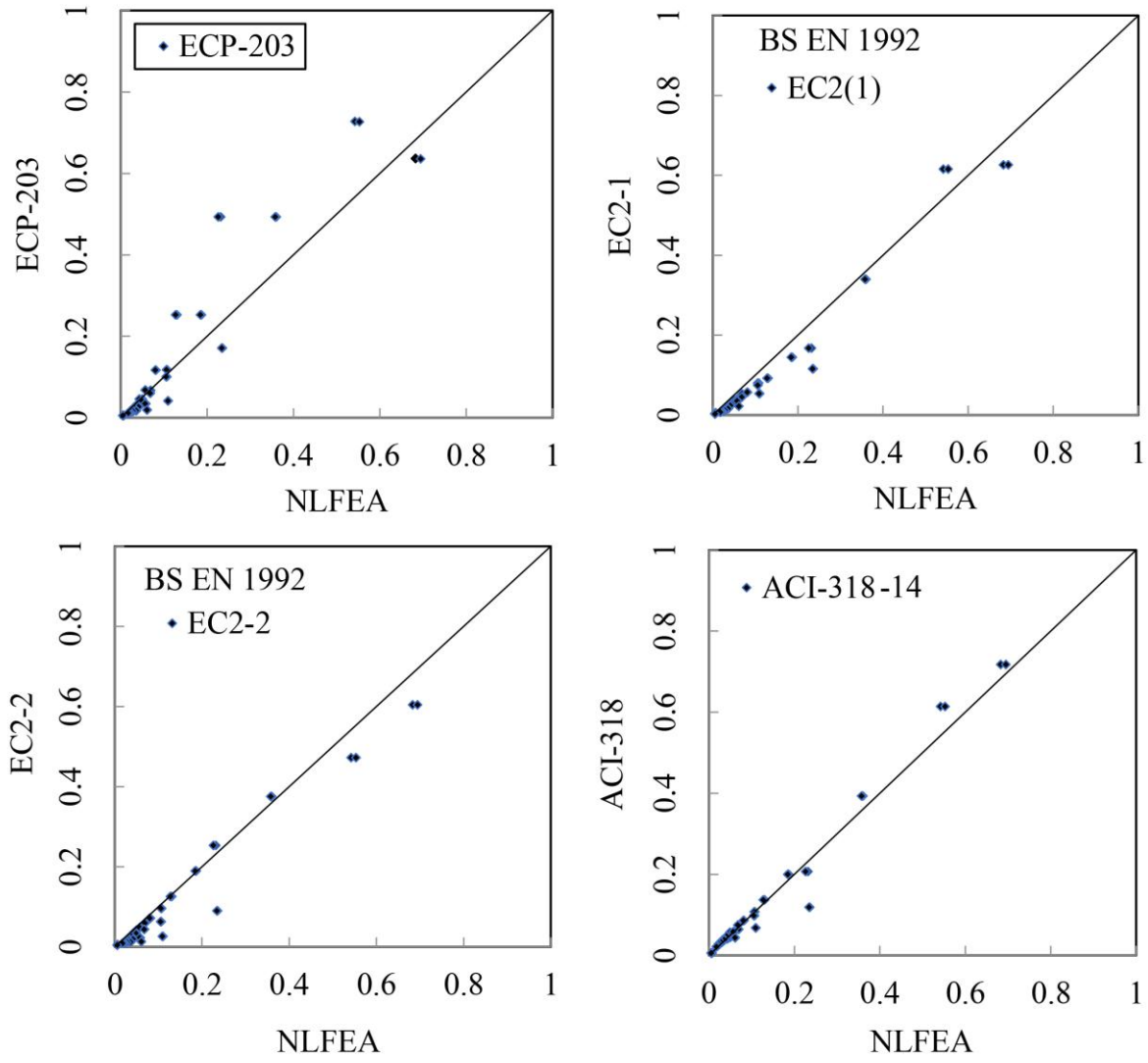

Figure 13

Accepted manuscript doi:
10.1680/jstbu.19.00064

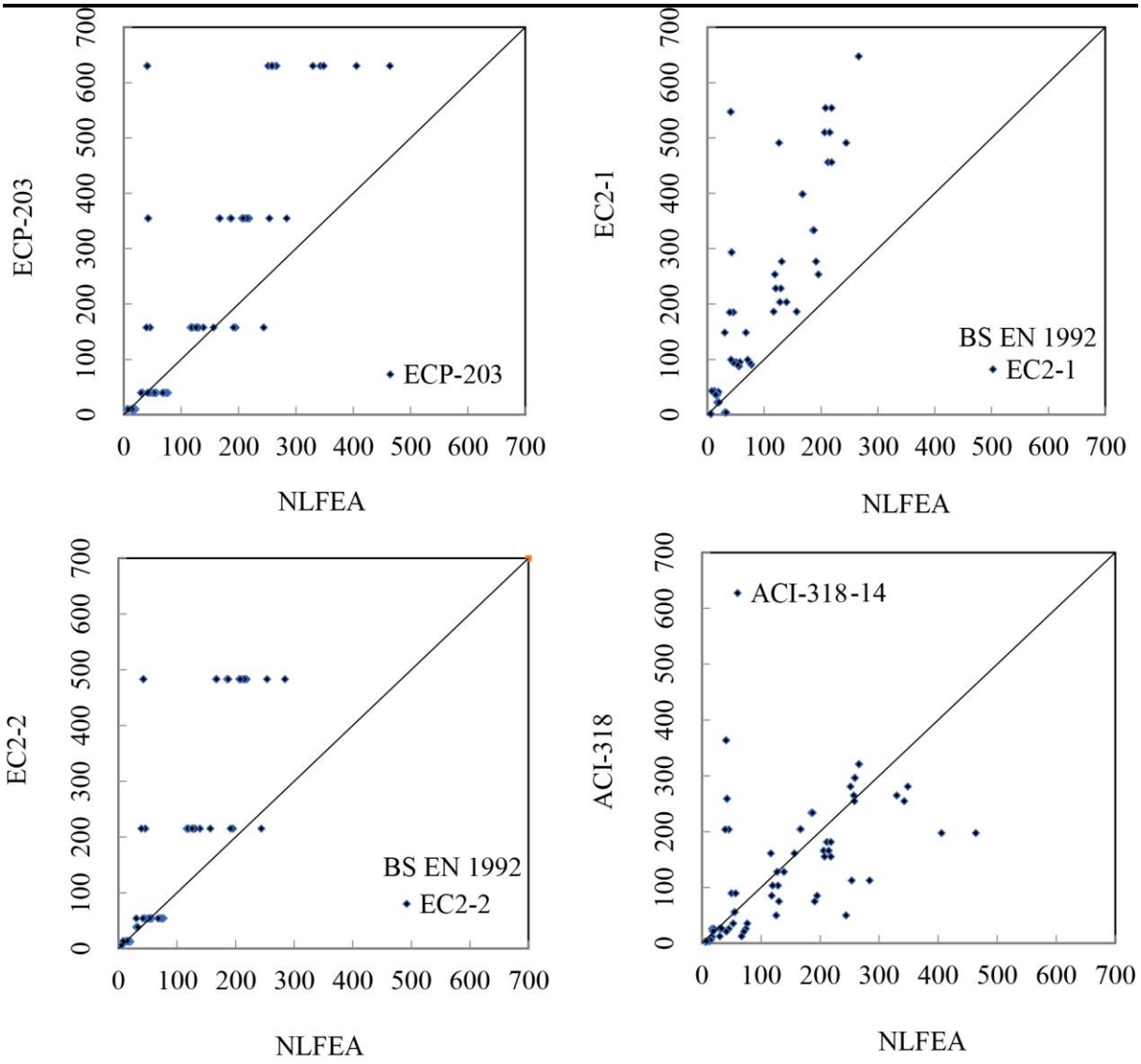

Figure 14

Accepted manuscript doi:
10.1680/jstbu.19.00064

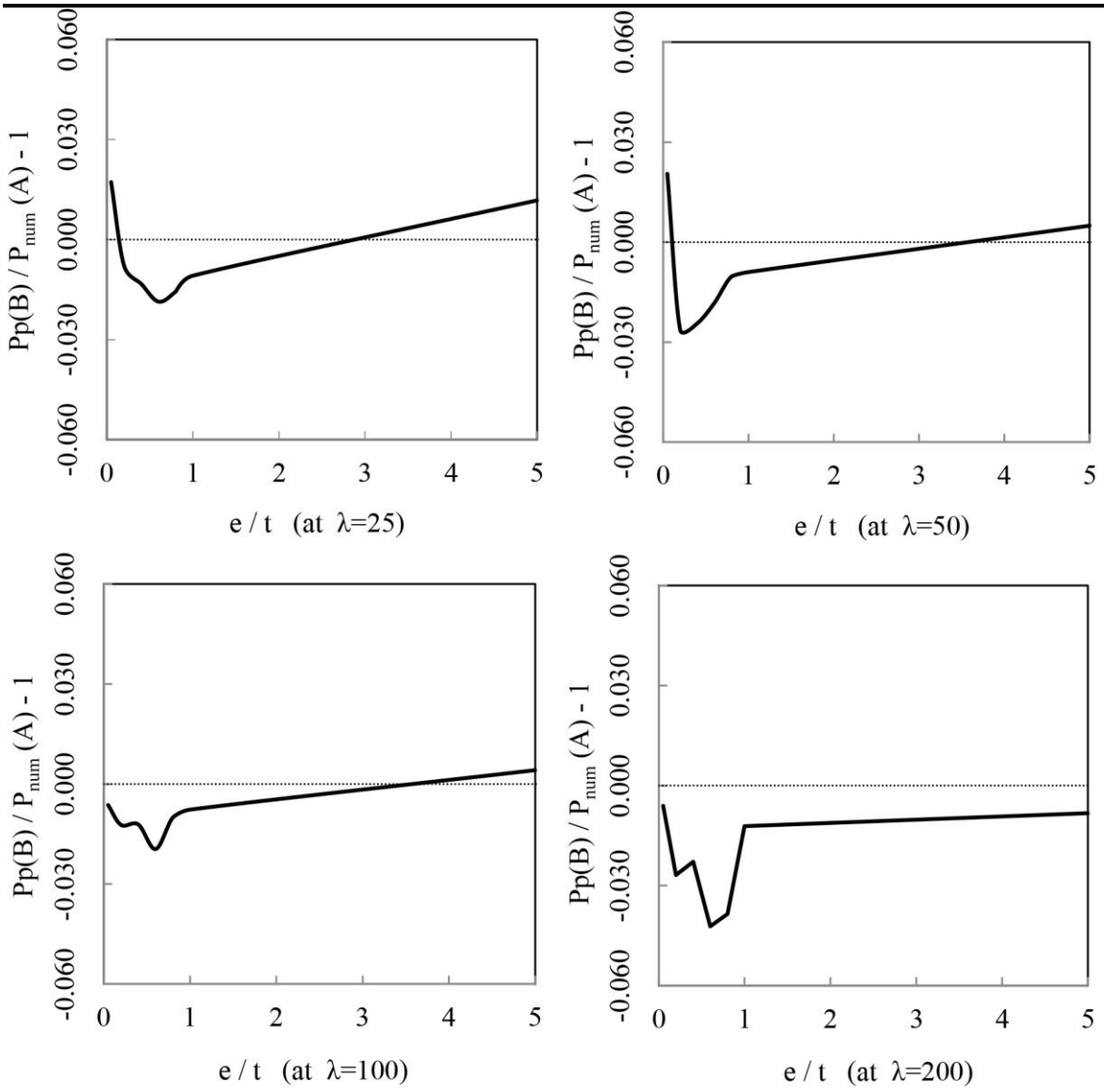

Figure 15

Accepted manuscript doi:
10.1680/jstbu.19.00064

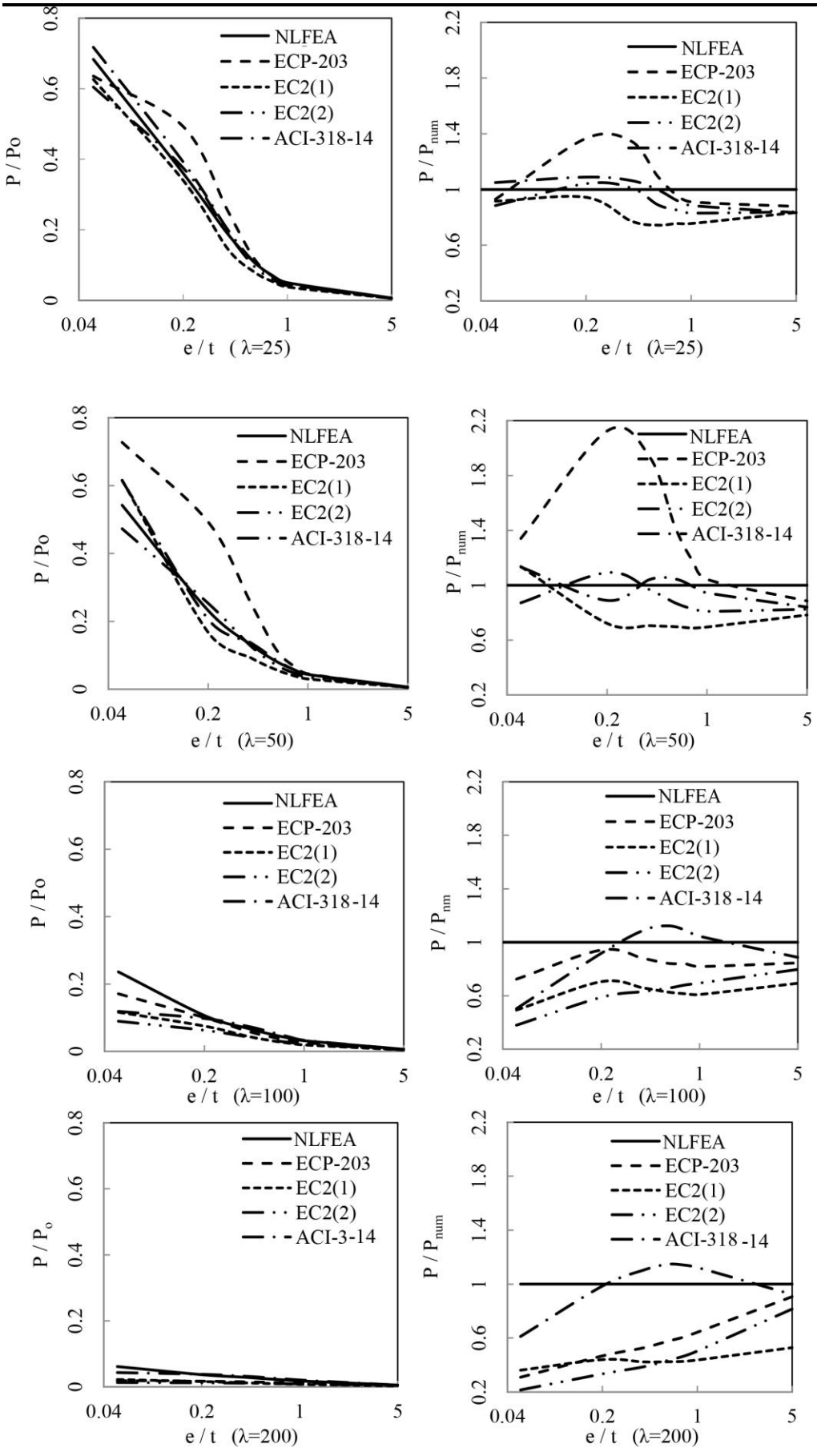

Figure 16

Accepted manuscript doi:
10.1680/jstbu.19.00064

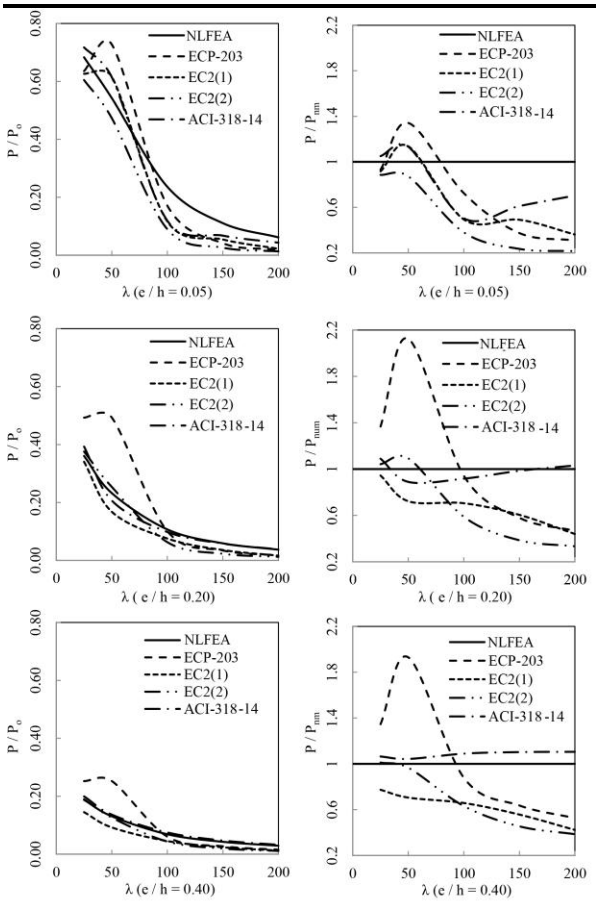

Figure 17

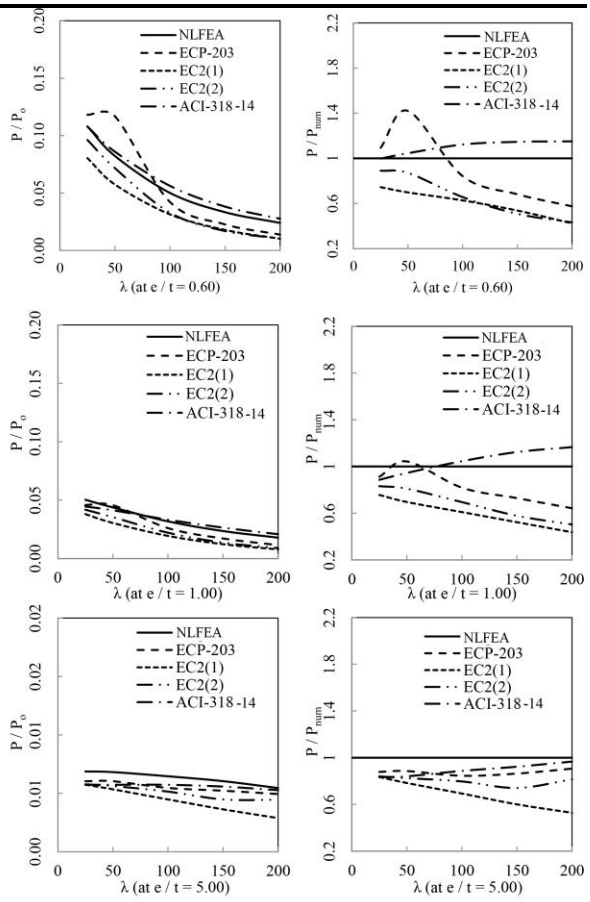

Figure 17

Accepted manuscript doi:
10.1680/jstbu.19.00064

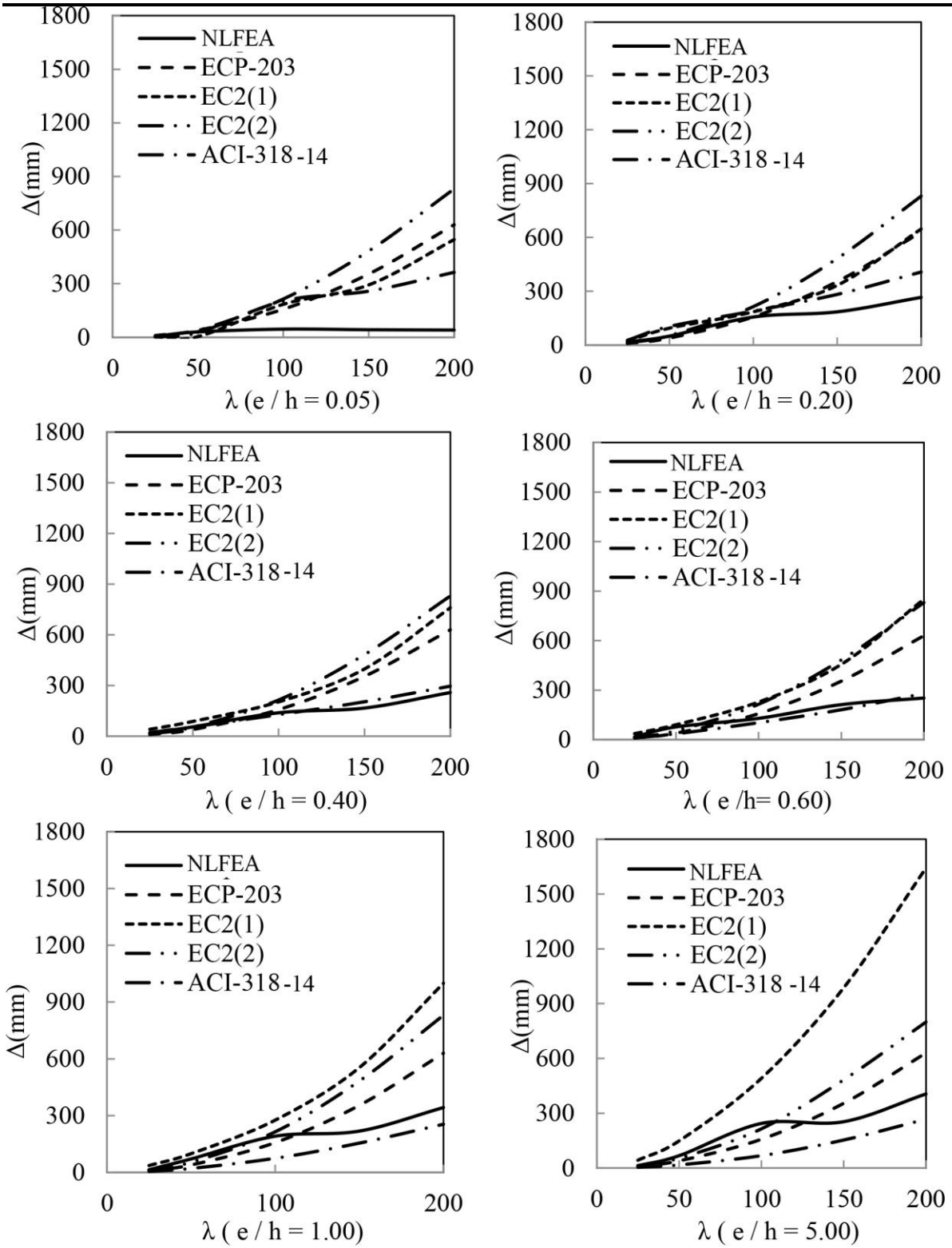

Figure 18

Accepted manuscript doi:
10.1680/jstbu.19.00064

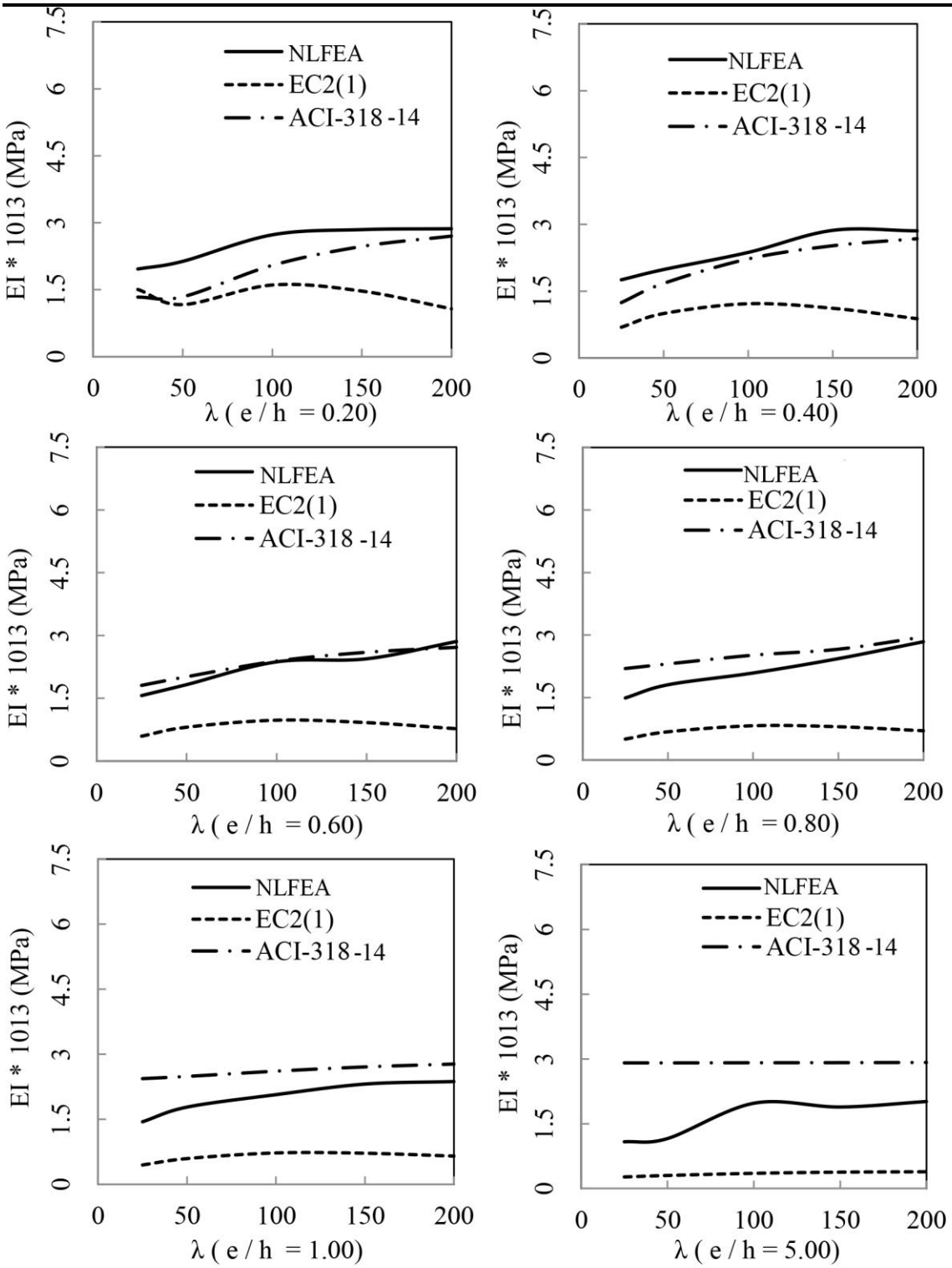

Figure 19